Thymosin beta 4 gene silencing decreases stemness and invasiveness in glioblastoma

Wirsching, Hans-Georg ; Krishnan, Shanmugarajan ; Florea, Ana-Maria ; Frei, Karl ; Krayenbühl, Niklaus ; Hasenbach, Kathy ; Reifenberger, Guido ; Weller, Michael ; Tabatabai, Ghazaleh

Abstract: Thymosin beta 4 is a pleiotropic actin-sequestering polypeptide that is involved in wound healing and developmental processes. Thymosin beta 4 gene silencing promotes differentiation of neural stem cells whereas thymosin beta 4 overexpression initiates cortical folding of developing brain hemispheres. A role of thymosin beta 4 in malignant gliomas has not yet been investigated. We analysed thymosin beta 4 staining on tissue microarrays and performed interrogations of the REMBRANDT and the Cancer Genome Atlas databases. We investigated thymosin beta 4 expression in seven established glioma cell lines and seven glioma-initiating cell lines and induced or silenced thymosin beta 4 expression by lentiviral transduction in LNT-229, U87MG and GS-2 cells to study the effects of altered thymosin beta 4 expression on gene expression, growth, clonogenicity, migration, invasion, self-renewal and differentiation capacity in vitro, and tumorigenicity in vivo. Thymosin beta 4 expression increased with grade of malignancy in gliomas. Thymosin beta 4 gene silencing in LNT-229 and U87MG glioma cells inhibited migration and invasion, promoted starvation-induced cell death in vitro and enhanced survival of glioma-bearing mice. Thymosin beta 4 gene silencing in GS-2 cells inhibited self-renewal and promoted differentiation in vitro and decreased tumorigenicity in vivo. Gene expression analysis suggested a thymosin beta 4-dependent regulation of mesenchymal signature genes and modulation of TGF and p53 signalling networks. We conclude that thymosin beta 4 should be explored as a novel molecular target for anti-glioma therapy.

DOI: https://doi.org/10.1093/brain/awt333

Thymosin β4 gene silencing decreases stemness and invasiveness in glioblastoma

Hans-Georg Wirsching,[1,4] Shanmugarajan Krishnan,[1,4] Ana-Maria Florea,[2] Karl Frei,[3,4] Niklaus Krayenbühl,[3] Kathy Hasenbach,[1] Guido Reifenberger,[2] Michael Weller,[1,4] Ghazaleh Tabatabai[1,4]

Laboratory of Molecular Neuro-Oncology of the [1]Departments of Neurology and [3]Neurosurgery, University Hospital Zurich, Zurich, Switzerland; [2]Department of Neuropathology, Heinrich Heine University Düsseldorf, Düsseldorf, Germany; [4]Neuroscience Center Zurich, University of Zurich and ETH Zurich, Zurich, Switzerland

Corresponding author:

Ghazaleh Tabatabai, MD PhD, Department of Neurology, University Hospital Zurich, Frauenklinikstrasse 26, 8091 Zurich, Switzerland; phone: +41-(0)44-255-5195, fax: +41-(0)44-255-4507; e-mail address: ghazaleh.tabatabai@usz.ch

Running title: Thymosin β4 in glioblastoma (27 characters)

ABSTRACT

Thymosin β4 (TB4) is a pleiotropic actin-sequestering polypeptide that is involved in wound healing and developmental processes. TB4 gene silencing promotes differentiation of neural stem cells whereas TB4 overexpression initiates cortical folding of developing brain hemispheres. A role of TB4 in malignant gliomas has not yet been investigated.

We analyzed TB4 staining on tissue microarrays and performed interrogations of the REMBRANDT and the TCGA databases. We investigated TB4 expression in 7 established glioma cell lines and 7 glioma-initiating cell lines and induced or silenced TB4 expression by lentiviral transduction in LNT-229, U87MG and GS-2 cells to study the effects of altered TB4 expression on gene expression, growth, clonogenicity, migration, invasion, self-renewal and differentiation capacity *in vitro*, and tumorigenicity *in vivo*.

TB4 expression increased with grade of malignancy in gliomas. TB4 gene silencing in LNT-229 and U87MG glioma cells inhibited migration and invasion, promoted starvation-induced cell death *in vitro* and enhanced survival of glioma-bearing mice. TB4 gene silencing in GS-2 cells inhibited self-renewal and promoted differentiation *in vitro* and decreased tumorigenicity *in vivo*. Gene expression analysis suggested a TB4-dependent regulation of mesenchymal signature genes and modulation of TGF-β and p53 signaling networks.

We conclude that TB4 should be explored as a novel molecular target for anti-glioma therapy.

Keywords: glioblastoma, thymosin β4, invasion, stemness

INTRODUCTION

Glioblastomas are highly aggressive primary brain tumors thought to originate from neural stem or progenitor cells (Chen *et al.* , 2012, Galli *et al.* , 2004, Liu *et al.* , 2010, Zheng *et al.* , 2008). Despite recent advances in multimodal treatment approaches including surgery, radiotherapy and chemotherapy, the median overall survival of glioblastoma patients is still poor, i.e. in the range of 16 months in selected clinical trial populations (Gilbert *et al.* , 2011, Stupp *et al.* , 2005) and approximately 11 months in population-based studies (Johnson and O'Neill, 2012). Recently, sub-groups of malignant gliomas have been defined according to gene expression signatures. Increased invasiveness and poor prognosis were found to be associated with a mesenchymal gene expression signature, whereas expression of genes associated with neural differentiation was associated with improved patient survival (Verhaak *et al.* , 2010). Furthermore, the expression of a mesenchymal gene signature was reported to be characteristic of a sub-population of glioma cells termed glioma stem-like or glioma-initiating cells (GIC) (Carro *et al.* , 2010). These cells are believed to promote malignancy and evasion from conventional therapies (Bao *et al.* , 2006, Chen *et al.* , 2012, Singh *et al.* , 2004). GIC exhibit features of neural stem cells (Galli *et al.* , 2004), and induction of differentiation in the GIC sub-population might be a potential therapeutic approach to glioblastoma.

Thymosin β4 (TB4) is the most abundantly expressed member of the β-thymosin family of small pleiotropic polypeptides. Beta thymosins were first isolated from calf thymus and thought to be thymic hormons (Low *et al.* , 1979). However, the first reported cellular function of β-thymosins was buffering of actin monomers (Safer *et al.* , 1990). To date, numerous functions beyond actin sequestering have been identified. For example, TB4 gene silencing in the heart led to a reduced number of mesenchymally differentiated cells and decreased migration of differentiated cells from the epicardial stem cell niche into the heart muscle, both during development and healing of ischemic wounds (Bock-Marquette *et al.* , 2004). Furthermore, TB4 activates epicardial stem cells and promotes reprogramming of cardiac fibroblasts to induced pluripotent stem cells (Qian *et al.* , 2012, Smart *et al.* , 2007). In the developing brain, TB4 expression is tightly associated

with neurogenesis and regulates expansion of the stem cell pool of the early neuroepithelium (Roth *et al.* , 1999, Wirsching *et al.* , 2012), whereas TB4 gene silencing promotes the differentiation of neural stem cells *in vitro* (Mollinari *et al.* , 2009). A role for TB4 has also been suggested in certain brain diseases. TB4 expression increased after focal brain ischemia (Vartiainen *et al.* , 1996) and after transient global hypoxia (Kim *et al.* , 2006) in the rat, while proteomic analysis showed increased TB4 protein levels in the cerebrospinal fluid (CSF) of patients with Creutzfeldt-Jakob disease (Mohring *et al.* , 2005). The pivotal role of TB4 in promoting cellular invasion and its role in brain development prompted us to investigate a putative involvement of TB4 in glioma pathogenesis.

MATERIALS AND METHODS

Tissue specimen and tissue microarray (TMA) construction

Immunohistochemical stainings for TB4 expression were performed on a tissue microarray (TMA) comprising 89 surgical glioma samples collected from patients who were treated at the Department of Neurosurgery, University Hospital of Zurich, Zurich, Switzerland between 06/2003 and 05/2009. All tumors were classified and graded according to the WHO classification of tumors of the central nervous system. For semi-quantitative analysis of TB4 staining intensity, we graded TB4 staining arbitrarily from 0-3 (0: negative, 1: weak, 2: moderate, 3: strong) for each tumor compartment, i.e. endothelial cells, inflammatory host cells and tumor cells. Compartments were identified based on morphology. Confirmatory immunohistological stainings were performed using antibodies against CD31 for endothelial cells, CD45 and CD11b for inflammatory host cells, and glial fibrillary acidic protein (GFAP) for tumor cells. In addition, we graded TB4 staining arbitrarily for each tissue sample from 0-3, based on the fraction of moderately or strongly TB4 positive cells (0: less than 20 %, 1: 20-50 %, 2: 50-80%, 3: more than 80% TB4 positive cells, respectively). Examples for weak/negative staining versus moderate/strong staining are given in Supplementary Fig. 1A.

Database interrogations

Publically available microarray and clinical data of glioma patients were acquired from the REpository for Molecular BRAin Neoplasia DaTa (REMBRANDT) using the data set available on May 19, 2011 (NCI, 2005) and from The Cancer Genome Atlas (TCGA) using the data set available on December 15, 2012 (McLendon *et al.* , 2008). Gene expression and Kaplan-Meier survival data were queried following the REMBRANDT site's instructions for "advanced search" and via the caINTEGRATOR homepage (https://caintegrator2.nci.nih.gov) following the site's instructions. The sample group for gene expression was restricted to WHO grade II/III gliomas (n = 184) and glioblastomas (n = 220). Survival data for the Kaplan-Meier analysis using the REMBRANDT database were retrieved for glioblastoma (n = 182). Samples with a

0.5-fold down-regulation or a 2-fold up-regulation of the target gene compared to median expression levels were defined as up- or down-regulated, the other samples were defined as intermediate.

Kaplan-Meier survival data from TCGA (n=465) were queried via the R2 microarray analysis and visualization platform (http://hgserver1.amc.nl/cgi-bin/r2/main.cgi). The averaged mRNA expression staining was scaled to 4775.5 for *TMSB4X* and 12.5 for *TMSB4Y*. The cut-off for the highest impact on survival was 7617.2 for *TMSB4X* and within the male population (n=311) 9.5 for *TMSB4Y*.

For analysis of functional gene interactions, combined confidence scores were generated for each putative interaction by integration of experimental and predicted data using the Search Tool for the Retrieval of Interacting Genes/Proteins (STRING) Version 9.0 at http://string-db.org (Szklarczyk *et al.* , 2011). Highest confidence settings were applied, thus merely integrating combined scores higher than 0.900. Cluster analysis was performed by application of the MCL algorithm.

Cell culture

LN-18, LNT-229 and LN-308 glioma cell lines were kindly provided by Dr. N. de Tribolet (Lausanne, Switzerland). T98G, U87MG and A172 glioma cell lines were purchased from the American Type Culture Collection (Manassas, VA). The TU159 cell line was generated in our laboratory (Bahr *et al.* , 2003). GS-2, GS-3, GS-4, GS-5, GS-7, GS-8 and GS-9 GIC lines were provided by Dr. Katrin Lamszus (Gunther *et al.* , 2008). All conventional cell lines were cultured in Dulbecco's modified Eagle's medium (DMEM) (Radnor, PA) containing 10% fetal calf serum (FCS), 2 mM glutamine and penicillin (100 IU/ml)/streptomycin (100 µg/ml). All GIC lines were cultured in Neurobasal-A medium supplemented with B27 (Invitrogen, Carlsbad, CA), 10 ng/ml basic fibroblast growth factor (bFGF), and 10 ng/ml epidermal growth factor (EGF) (BD Biosciences, Franklin Lakes, NJ). Growth factors were replenished twice weekly. Conditioned supernatants were generated by seeding 2 million cells in T75 flasks overnight, then washing three times and adding serum-free DMEM for conditioning for 72 h.

Lentiviral constructs

An shRNA expression cassette for targeting TB4 or a scrambled sequence were cloned into a custom-made *SEW*-based lentivirus (Demaison *et al.* , 2002) under control of the *U6*-promoter. For targeting TB4, the following sequences were used: 5'-CTGAGATCGAGAAATTCGATAAG-3' which is highly conserved and orthologue in mouse and human *TMSB4X* (Smart *et al.* , 2007) and the sequence 5'-TGGCTGAGATCGAGAAATT-3' (si_2). Both constructs were designed to co-express monomeric dsRed under the control of the *SFFV*-promoter to assess the efficacy of stable transduction. The original GFP cassette from the SEW vector was excised. For TB4 overexpression, the coding sequence of *hTMSB4X* was cloned into a custom-made *SEW*-based lentivirus under the control of the *SFFV*-promoter (Demaison *et al.* , 2002), followed by the coding sequences of an 2A-autocleavage site, monomeric dsRed and *WPRE*. Lentivirus was produced and titred (Tabatabai *et al.* , 2010) and target cells were transduced at a multiplicity of infection (MOI) of 100 transducing lentiviral particles per cell.

Quantitative reverse transcriptase PCR

Total RNA was prepared using the NucleoSpin System (Macherey-Nagel, Düren, Germany) and cDNA transcribed using Superscript II reverse transcriptase (Invitrogen). For real-time PCR, cDNA amplification was monitored using SYBRGreen chemistry on the 7300 Real time PCR System (Applied Biosystems, Zug, Switzerland). The conditions for these PCR reactions were: 40 cycles, 95°C/15 sec, 60°C/1 min, using the following specific primers: Arf1 fwd: 5'- GACCACGATCCTCTACAAGC-3', Arf1 rv: 5'-TCCCACACAGTGAAGCTGATG-3'; TB4 fwd: 5'-AAACCCGATATGGCTGAGAT-3', TB4 rv: 5'-TGCTTCTCCTGTTCAATCGT-3', TB15A fwd: 5'-GCCTCCCAACAGCAGATTTCGA-3', TB15A rv: 5'-ACAGCATCTGCCATCTGGAACA-3', TB15B fwd: 5'-TCCTCCAAAGAGCAGATTTCAG-3', TB15B rv: 5'-GCATCTGCCATTTGGAATTTACA-3', TGFB1 fwd: 5'-GCCCTGGACACCAACTATTG-3', rev: 5'-CGTGTCCAGGCTCCAAATG-3', TGFB2 fwd: 5'- AAGCTTACACTGTCCCTGCTGC-3', rev: 5'-TGTGGAGGTGCCATCAATACCT-3'. Arf1 transcript levels were used as a house-keeping reference for

relative quantification of mRNA expression levels using the ΔC_T method. The samples for normal brain cDNA were purchased from Ambion (Ambion, Applied Biosystems, Foster City, CA).

Reporter assay

TGF-β-induced signalling was assessed by reporter assays using the SMAD-binding elements (SBE) containing reporter plasmid pGL3-SBE4-Luc (Zawel *et al.* , 1998) kindly provided by Dr. B. Vogelstein (Baltimore, MD), and the TGF-β-responsive plasminogen activator inhibitor 1 promoter fragment containing the reporter plasmid pGL2-3TP-Luc (Wrana *et al.* , 1992), which was kindly provided by Dr. J. Massague (New York, NY). Dual luciferase/renilla assays were performed with co-transfection of 150 ng of the respective reporter construct and 20 ng of pRL-CMV. Luciferase activity was measured using a Mithras LB 940 microplate reader (Berthold, Bad Wildbad, Germany) and normalized to constitutive renilla activity (pRL-CMV).

Immunoblot analysis

Denatured whole protein lysates (20 µg/lane) were separated on 10-13% acrylamide gels. After transfer to nitrocellulose (Biorad, Hercules, CA), blots were blocked in PBS containing 5% skim milk and 0.05% Tween 20 and incubated overnight at 4°C with primary antibodies, washed in PBS and incubated for 1 h at room temperature with secondary antibodies. Primary antibodies were anti-TB4 (Immundiagnostik, Bensheim, Germany), anti-ILK (Lab Force, Nunningen, Switzerland) and anti-(p)Akt (Bioconcept, Allschwil, Switzerland). Visualization of protein bands was accomplished using horseradish peroxidase-coupled secondary antibodies (Santa Cruz Biotechnology, Santa Cruz, CA) and the enhanced chemiluminescence (ECL) technique (Thermo Fisher Scientific).

Enzyme-linked immunosorbent assay (ELISA)

Conditioned supernatants were generated as described above. Next, 1N HCl was added for 20 min to activate latent TGF-β. TGF-β_1 and TGF-β_2 protein levels were assessed by a commercially available ELISA kit (R&D Systems). Streptavidine-horseradisch peroxidase was added for 20 min, then after washing substrate solution was added for another 20 min and optical density was measured at 450 nm using a Mithras LB 940 microplate reader (Berthold). The standard curve was calculated using recombinant TGF- β_1 and TGF-β_2 at pre-defined concentrations, and a computer generated 4-PL curve-fit (Excel, Microsoft, Seattle, WA).

Flow cytometry

All flow cytometry analyses were performed using a CyAN ADP flow cytometer (Beckman Coulter, Brea, CA). For cell cycle analysis, cells were washed, resuspended in PBS and fixed by slowly adding ice-cold ethanol to a final concentration of 70% and incubation on ice for 60 min. Cells were washed and resuspended in buffer (PBS containing 0.5% BSA, 0.02% NaN3, 1 mM EDTA) at 100,000 cells per 30 µl. Cells were incubated with 5 µl of a custom-made stock solution containing 2.5 mg/ml propidium iodide (Sigma-Aldrich, St. Louis, MO), 0.1 mg/ml RNaseA (Roth, Karlsruhe, Germany) and 0.05% Triton X-100 (Sigma-Aldrich) for 30 min at 4°C and subsequently washed and resuspended in buffer. For separation of cells by DNA content, a PE laser was used to measure the peak plane. For annexinV-PI analysis, cells were stained with propidium iodide (Sigma-Aldrich) and pacific blue-labelled annexinV (Lucerna, Lucerne, Switzerland).

MMP activity assay

For assessment of MMP activity, the FRET-based SensoLyte 520 MMP Substrate Sampler Kit (Anaspec, Fremont, CA) was used. In brief, conditioned supernatants of LNT-229 glioma cells were incubated with the substrate QXL520^{TM}-γ-Abu-Pro-Cha-Abu-Smc-His-Ala-Dab(5-FAM)-Ala-Lys-NH238 (Smc=S-Methyl-L-cysteine). Fluorescence emission was measured in a Mithras LB 940 microplate reader (Berthold) at Ex/Em=490 nm/535 nm. A standard curve for quantification was obtained using the pre-cleaved fragment 5-FAM-Pro-Leu-OH at predefined concentrations.

Affymetrix gene chip analysis

Total RNA was extracted from LNT-229 and U87MG glioma cell lines transfected either with siTB4 or scrambled control siRNA using the RNeasy Kit (Qiagen, Hilden, Germany). High RNA quality, as indicated by RNA integrity numbers of >9, was assured by using the Agilent 2100 Bioanalyzer (Agilent, Böblingen, Germany). RNA samples were processed using the 3'IVT express kit (Affymetrix, Santa Clara, CA) starting from a total amount of 100 ng RNA. Labeled cRNA was hybridized to Affymetrix GeneChip Human genome U133 2.0 plus arrays, followed by washing, labeling and scanning according to standard protocols. The GeneSpring software (Agilent) was used for determination of normalized gene expression values.

Growth, Alamar blue, clonogenicity and sphere formation assays

For growth assays, 1,000 LNT-229 or U87MG cells, or 5,000 GS-2 cells per well were seeded in 24-well plates and triplicates were counted daily. Viable cells were identified using trypan blue dye exclusion.

For Alamar blue assays (Invitrogen), 1,000 cells were seeded in 96-well plates and supplemented with 10% Alamar blue for 1 h. Fluorescence emission of metabolized Alamar blue was measured in a Mithras LB 940 microplate reader (Berthold at Ex/Em=560 nm/600 nm). For clonogenic survival assays of LNT-229 or U87MG, 500 cells were seeded in triplicate in 6-well plates. After 20 days, cells were stained using 0.5% crystal violet solution. Colonies of 50 or more cells were counted manually at 10x magnification.

For sphere formation assays, GS-2 cells were initially separated from each other mechanically and with accutase (Chemie Brunschwig, Bale, Switzerland). Cells were then seeded in neurobasal medium supplemented with growth factors in 6-well plates at a density of 1 cell per 4 µl and sphere formation was assessed by manually counting spheres at 10x magnification after 20 days. Sphere volume was calculated based on diameters of spheres assessed in 12 high power fields using ImageJ 1.40g software (NIH, Bethesda, MD).

Migration and invasion assays

Migration of glioma cells was measured in transwell migration assays (24 wells, 8 µm pore size; BD Biosciences). In brief, 5 x 10^4 cells in 200 µl serum-free DMEM (SFM) were added to each transwell insert. NIH 3T3-conditioned medium (700 µl) was used as a chemoattractant in the lower wells. NIH 3T3 fibroblasts secrete a variety of growth factors, and therefore the conditioned medium from these cells is commonly used as a chemoattractant (Albini *et al.* , 1987). After an incubation period of 16 h, the cells on the lower side of the membrane were fixed in ice-cold methanol at 4°C, stained with hemalaun, and sealed on slides. Quantification of cell migration was expressed as the mean count of stained cells in eleven random fields of each membrane.

For invasion assays, glioma spheroids were generated by incubating 1,000 cells for 72 h in 96-well plates precoated with 1% Noble Agar (Difco Laboratories, Detroit, MI). Spheroids with a diameter of approximately 200 µm were embedded into a collagen matrix containing collagen type I (Invitrogen), 10% FCS and 10% $NaHCO_3$ in a 96-well plate. Sprouting of spheroids was monitored by daily photographs or by time-lapse video microscopy using a JuLI image viewer (NanoEnTek, Seoul, Korea). For quantitation, the area covered by sprouting cells and the median invaded distance of 50 cells were assessed using the ImageJ 1.40g software (NIH). The spheroid margin at day 0 was used as a reference point for measurement of the invaded distance of sprouting cells. For measurement of the invasion area, the area covered by the spheroid at day 0 was subtracted from the overall area that was covered on subsequent days.

Differentiation assay

For the induction of differentiation, GIC were cultured in full neurobasal medium supplemented with the indicated FCS concentrations for 5 days. Differentiation was assessed by counting cells that exhibited an adherent phenotype and by immunostaining for glial fibrillary acid protein (GFAP) or nestin.

Animal studies

All experiments were performed according to the Swiss animal protection law. CD1$^{nu/nu}$ mice were purchased from Charles River Laboratories (Wilmington, MA). Mice aged 8–12 weeks were anesthetized and placed in a stereotaxic fixation device. A burr hole was drilled in the skull 2 mm lateral and 1 mm posterior to the bregma. The needle of a Hamilton syringe was introduced into a depth of 3 mm (Tabatabai *et al.* , 2007). LNT-229 (75 x 10^4), U87MG (10^5) or GS-2 (2 x 10^5) cells were resuspended in PBS and were injected into the right striatum. GS-2 cells were dissociated prior to injection. Animal experiments with LNT-229 gliomas were performed twice. Animal experiments with U87 and GS-2 gliomas were performed once. Animals were assessed clinically thrice weekly and were sacrificed at a clinical score of 2 (Supplementary Table 1).

Immunocytology, histology and immunohistochemistry

Primary antibodies were monoclonal mouse anti-Nestin (Zytomed, Berlin, Germany, 1:100), polyclonal rabbit anti-GFAP (Dako, Glostrup, Denmark, 1:1000), monoclonal mouse anti-NeuN (Chemicon, Temecula, CA, 1:100), polyclonal rabbit anti-β-III-Tubulin (R&D Systems, Minneapolis, MN), monoclonal mouse anti-CD31 (Dako, Glostrup, Denmark, 1:50), monoclonal mouse anti-CD45 (Dako, Glostrup, Denmark, 1:50), polyclonal rabbit anti-CD11b (Abcam, Cambridge, UK, 1:50) and polyclonal rabbit anti-Thymosin β4 (Immundiagnostik, Bensheim, Germany, 1:100). For immunocytochemistry, cells were grown on Poly-D-Lysine-coated cell culture slides (BD Biosciences) and fixed in PFA. Neurospheres were centrifuged onto glass slides using a Shandon Cytospin 4 (Thermo Fisher Scientific, Waltham, MA), dried briefly and fixed in PFA. Cells were permeabilized with 0.2% Triton X-100 and 10% normal horse or swine serum (Vector, Burlingame, CA) was used for blocking. For conventional histology, 5 µm paraffin sections were stained with hematoxylin & eosin. For immunohistochemistry, deparaffinized and rehydrated sections were boiled in EDTA buffer, pretreated with 1% H_2O_2, blocked in 10% swine serum or blocking solution (Candor Biosciences, Wangen, Germany). Biotinylated secondary antibodies, streptavidine and diaminobenzidine were obtained from Dako and used according to standard procedures.

Statistics

Quantitative data are expressed as mean or median and SEM, as indicated. For column statistics, unpaired t-test or one-way ANOVA followed by Tukey's post hoc test was performed. The *in vitro* experiments reported here were performed at least three times in triplicate with similar results. For survival statistics Gehan-Breslow-Wilcoxon test was performed. All statistical analyses were performed using Prism 5 (GraphPad Software, La Jolla, CA).

RESULTS

TB4 is overexpressed in malignant gliomas

We investigated TB4 levels in malignant gliomas *in vivo* by immunohistochemistry on a TMA containing tissue cores from 89 gliomas of different WHO grades (17 WHO grade II, 24 WHO grade III, 48 WHO grade IV) and 4 normal brain tissue control samples. Representative stainings are shown in Figure 1A. The highest TB4 levels were observed in glioblastomas (Fig. 1B). We analyzed TB4 staining in 3 different compartments, i.e. tumor cells, inflammatory host cells and endothelial cells (Supplementary Fig. 1A-D). This compartment-specific analysis revealed a correlation of TB4 staining intensities with increasing WHO grade in tumor cells (Fig. 1C), but not in inflammatory host cells or endothelial cells (Supplementary Fig. 1C and D). In glioblastoma samples, the TB4 staining intensity was higher in tumor cells than in host or endothelial cells (Fig. 1D). We also correlated TB4 staining data with clinical parameters (Supplementary Table 2). In glioblastomas, TB4 levels did not differ between younger versus older patients (Supplementary Fig. 1E), but TB4 levels were higher in recurrent vs primary glioblastomas (Supplementary Fig. 1F). For correlation with clinical outcome, we subdivided samples by low (0-2) versus high (>2) arbitrary TB4 levels. Median overall survival was lower in the group of patients with strongly TB4 positive glioblastomas (TB4 low: 15.1 months vs TB4 high: 9.9 months, $p<0.05$) (Fig. 1E). A more detailed investigation of TB4 staining and its role for clinical outcome in histological glioma subtypes of WHO grades II or III was precluded because of sample size.

To expand and validate our immunohistochemical TB4 data in malignant gliomas, we performed a REMBRANDT database interrogation (NCI, 2005). TB4 mRNA expression in gliomas correlated with increasing WHO grade (Supplementary Fig. 1G) and glioblastoma patients with low (<0.5-fold of median) TB4 expressing tumors had longer overall survival than patients with high (>2-fold of median) TB4 expressing glioblastomas (Fig. 1F). Correlation of TB4 expression with survival in glioblastoma was further confirmed by a TCGA database interrogation (Supplementary Fig. 1H).

Considering that the gene coding for TB4 is located on the X-chromosome prompted us to further analyze gender differences and expression of the homologous gene *TMSB4Y*. REMBRANDT and TCGA analyses yielded no differences of *TMSB4X* expression in female or male patients. Moreover, *TMSB4Y* was expressed, if at all, only at very low levels in both datasets, although with a significant correlation to survival in the male population (data not shown).

Next, we analyzed TB4 mRNA expression in 7 established glioma cell lines (T98G, U87MG, LN-18, LNT-229, LN-308, A172, Tu159) and in 7 GIC cultures (GS-2, GS-3, GS-4, GS-5, GS-7, GS-8, GS-9) using real-time RT-PCR analysis. TB4 was overexpressed up to 10-fold in all GIC cultures except for GS-4 and up to 22-fold in all long-term glioma cell lines relative to normal brain tissue samples used for reference (Supplementary Fig. 2). Immunocytochemistry indicated nuclear and cytoplasmic localization of TB4 in glioma cells, with a specific increase in cytoplasmic protrusions (Fig. 1G).

TB4 gene silencing in glioma cells enhances apoptotic cell death and decelerates clonogenic growth

To investigate the biological role of TB4 functions in glioma cells, we performed lentiviral shRNA-mediated gene silencing (siTB4) in two cell lines with low and high TB4 expression levels, i.e. LNT-229 and U87MG (Supplementary Fig. 2, Fig. 2A-B). Assessment of dsRed co-expression revealed lentiviral transduction efficacies close to 100% (Supplementary Fig. 3). TB4 gene silencing did not affect the mRNA expression levels of thymosin β15 (TB15), another member of the β−thymosin family (data not shown), thus validating the specificity of the shRNA sequence used for targeting TB4 and excluding compensatory upregulation of TB15. In addition, we overexpressed TB4 in LNT-229 and U87MG cells by lentiviral vectors (Supplementary Fig. 4A).

The growth of LNT-229 cells was increased upon TB4 overexpression (Supplementary Fig. 4B) and decreased after TB4 gene silencing (Supplementary Fig. 4C), resulting in doubling times during exponential growth of 20.2 h for TB4-overexpressing cells, as compared to 22.1 h for empty vector control cells, and 25.6

h for siTB4 cells, as compared to 21.0 h for scr cells. Reduced growth of LNT-229 cells depleted of TB4 was paralleled by reduced metabolic activity (Supplementary Fig. 4D).

One of the key features of cancer cells is survival under nutrient-restricted conditions (Hanahan and Weinberg, 2011). Thus, we analyzed cell viability by trypan blue exclusion in LNT-229 and U87MG glioma cells after 7 days of serum deprivation. Trypan blue-positive cells, i.e. the dead cell fraction was increased upon TB4 gene silencing (Fig. 2C). The effect of TB4 gene silencing on cell death under nutrient-restricted conditions was confirmed using a second shRNA sequence (Supplementary Fig. 5A-D). Flow cytometry-based analysis of the cell cycle indicated a 5-fold increase of the sub-G0/1 fraction in siTB4 cells whereas the cell cycle distribution upon starvation in the viable cell fractions was similar in both scr and siTB4 LNT-229 cells (Fig. 2D and E). In serum-containing cell culture medium, however, dead cell fractions did not differ in scr and in siTB4 cells. We then performed annexinV and PI flowcytometry in scr and siTB4 glioma cells to analyze whether enhanced starvation-induced cell death of TB4-depleted cells was paralleled by an increase in apoptosis. The percentage of apoptotic, i.e. annexinV-positive cells was 3.2-fold (48% vs 15%) higher in LNT-229 siTB4 and 2.2-fold (61% vs 28%) higher in U87MG siTB4 cells. The percentage of dead, i.e. PI-positive cells was 3.9-fold (43% vs 11%) higher in LNT-229 siTB4 and 2.6-fold (55% vs 21%) higher in U87MG siTB4 cells (Fig. 2F).

Next, we analyzed clonogenicity, single colony morphology and actin filament staining in LNT-229 scr and siTB4 cells (Fig. 2G-L). After TB4 gene silencing, the number of colonies was not reduced, but single colonies were smaller (Fig. 2G and J) and more compact (Fig. 2H and K) and cellular protrusions were reduced in size and number (Fig. 2I and L). Similar data were observed in U87MG (data not shown).

TB4 gene silencing inhibits migration and invasion of glioma cells *in vitro*

The accumulation of TB4 in cytoplasmic protrusions (Fig. 1G) and the marked reduction of size and number of cytoplasmic protrusions in LNT-229 siTB4 cells (Fig. 2L) prompted us to investigate the effects of TB4 on migration and invasion in LNT-229 and U87MG cells. We analyzed the invasiveness of LNT-229 scr or

siTB4 spheroids (Fig. 3A and B, Supplementary Fig. 5E and F), and U87MG scr or siTB4 spheroids (Fig. 3C and D, Supplementary video) in a three-dimensional collagen spheroid invasion assay and assessed invasion after 24 h (Fig. 3 E-H, Supplementary Fig. 5G and H) and after 48 h (Fig. 3I-L, Supplementary Fig. 5I and J) in a serum-containing collagen matrix. The area covered by invading cells was reduced by 2.7-fold in LNT-229 siTB4 and by 4.2-fold in U87MG siTB4 cells (Fig. 3M). The invaded distance was reduced by 2.3-fold in LNT-229 siTB4 and by 4.1-fold in U87MG siTB4 cells (Fig. 3N). Similar results were observed after targeting TB4 with a second shRNA sequence in LNT-229 (Supplementary Fig. 5K and L). Transwell migration of LNT-229 and U87MG cells was decreased upon TB4 gene silencing and increased upon TB4 overexpression (Supplementary Fig. 6), but no effect of TB4 overexpression on spheroid invasion was observed (data not shown).

TB4 gene silencing prolongs symptom-free survival of glioma-bearing mice *in vivo*

We orthotopically implanted LNT-229 or U87MG scr or siTB4 cells into nude mice. The latency until the onset of neurological symptoms was prolonged in animals bearing TB4-depleted experimental gliomas (Fig. 4A and B). The median time interval until the onset of symptoms was increased from 44 to 56 days ($p<0.05$) in LNT-229 glioma-bearing animals, and 45 to 54 days ($p<0.05$) in U87MG glioma-bearing animals. Histological analysis revealed smaller and less invasive tumors in siTB4 gliomas, and tumor volume was markedly reduced to approximately 20-30% at day 28 (Fig. 4C). At the onset of neurological symptoms, however, tumor size was similar in LNT-229 scr and siTB4 gliomas (Supplementary Fig. 7).

A TB4-dependent transcriptional network involves modulation of TGF-β signaling and regulates mesenchymal signature genes in glioma cells

Next, we aimed at analyzing the mechanism by which TB4 exerts its effects in glioma cells. First, we assessed integrin-linked kinase (ILK), Akt and matrix metalloproteinase (MMP)-2 expression after TB4 knockdown, because stabilization of ILK, phosphorylation of Akt and consecutive regulation of MMP2

expression by TB4 have been suggested in other cell types (Bock-Marquette *et al.* , 2004, Fan *et al.* , 2009). ILK protein levels were not decreased in LNT-229 siTB4 glioma cells and there was no effect of TB4 gene silencing on Akt phosphorylation on Ser473 (Supplementary Fig. 8A). We reasoned that phosphoinositide 3-kinase (PI3K) signaling might compensate for effects of siTB4 on ILK levels, because PI3K is a major ILK activator. Indeed, upon treatment with the PI3K inhibitor wortmannin ILK protein levels were reduced in TB4-depleted cells, but with yet no effect on Akt phosphorylation. MMP2 protein levels remained unaffected upon TB4 gene silencing, too (Supplementary Fig. 8B), but MMP-activity was reduced in an assay that detects the activity of multiple MMP (MMP 1/2/3/7/8/9/12/13/14) (Supplementary Fig. 8C). These results indicate that TB4 stabilizes ILK in glioma cells and alters MMP activity, but does not affect Akt phosphorylation.

To understand the molecular network controlled by TB4 in glioma cells, we performed an Affymetrix chip-based transcriptome analysis of LNT-229 scr and siTB4 cells and retrieved a list of regulated candidate genes. At a 2.0 fold-change cut-off, 1.724 probe sets were differentially detected, including 162 that were directed against a total of 116 cDNAs coding for transcription factors (Supplementary Table 3). Submission of all differentially expressed transcription factors to the Search Tool for the Retrieval of Interacting Genes/Proteins (STRING) identified 2 main clusters (Fig. 5A). One cluster involved mainly genes interacting with *TP53* (green nodes), the other cluster was centered around the downstream TGF-β signaling modulators *EP300* and *FOS* (red nodes). The latter cluster furthermore comprised the TGF-β signaling modulators *CITED1* and *CITED2*, and interacted with a third cluster comprising the TGF-β signaling modulators *SMAD6* and *SMAD7* (brown nodes). All 6 identified TGF-β signaling modulators were downregulated in the Affymetrix gene chip in siTB4 glioma cells.

As we had observed enhanced apoptosis and decreased migration and invasion upon TB4 gene silencing (Figs. 2 and 3, Supplementary Fig. 5), we performed a gene ontology (GO) analysis with TB4-dependently differentially regulated genes. GO annotation identified 34 genes involved in migration (Supplementary Table 4) and 75 genes involved in apoptosis (Supplementary Table 5), with an overlap of 14 genes that are

annotated to both processes, including the TGF-β signaling modulators *TGFB2, THBS1*, *CITED 2* and *SMAD7*. Furthermore, inhibitors of TGF-β signaling including *ONECUT2* and *FBN1* were up-regulated in LNT-229 siTB4 cells. Conversely, TGF-β signaling transcriptional target genes including *SNAI2, IRX1, FBXO32, DAPK1, ATG5, ATG7, TGFA, PDGFC, COL1A2* and *FN1* were downregulated upon TB4 gene silencing.

The central role of TGF-β signaling in gliomas prompted us to further validate it by qRT-PCR, ELISA and reporter assays. *TGFB1* mRNA levels were reduced in LNT-229 siTB4 cells by 2.2-fold and in U87MG siTB4 cells by 3.6-fold (Supplementary Fig. 9A). *TGFB2* mRNA levels were reduced in LNT-229 siTB4 cells by 4.3-fold and in U87MG siTB4 cells by 18.3-fold, respectively (Supplementary Fig. 9B). The levels of TGF-β_1 and TGF-β_2 protein in the supernatants of LNT-229 siTB4 were decreased by 1.4-fold and 4.5-fold, respectively (Supplementary Fig. 9C and D). Furthermore, decreased TGF-β signaling in LNT-229 siTB4 was confirmed using a dual luciferase/renilla reporter assay (Supplementary Fig. 9E).

Inhibition of TGF-β signaling inhibits stem cell properties and promotes a more differentiated gene expression pattern of glioma cells due to decreased expression of the Sry-related HMG-box factor SOX2 (Ikushima *et al.* , 2009) and *SOX2* was down-regulated in TB4-depleted LNT-229 cells (Supplementary Table 3). Thus, we compared the expression signature of TB4-depleted cells with recently established signatures of gliomas that take into account levels of differentiation (Carro *et al.* , 2010, Freije *et al.* , 2004, Phillips *et al.* , 2006, Verhaak *et al.* , 2010). A comparison of the signature of TB4-depleted cells with the signatures suggested by Freije and colleagues (2004) revealed up-regulation of the neurogenesis signature genes *BMP2* and *HEY2*, whereas the invasive signature genes *COL6A3*, *THBS1* and *FN1* and the proliferative signature genes *TOP2A, CDKN3, PTTG1* and *CENPF* were down-regulated (Freije *et al.* , 2004). A comparison with the signatures suggested by Phillips and colleagues (2006) revealed an up-regulation of the proneural signature gene *GABBR1,* silencing of the marker genes of the proliferative signature *IQGAP3* and *HMMR* and silencing of the mesenchymal signature genes *COLA4A1* and *COL4A2* (Phillips *et al.* , 2006). Of note, gene silencing of *IQGAP3*, *HMMR, COLA4A1* and *COL4A2* is also a feature of the proneural signature, as defined

by the centroids of k-means clustering (Phillips et al. , 2006). A shift of the mRNA expression pattern of LNT-229 siTB4 cells towards a proneural signature was furthermore apparent when comparing the TB4-depletion signature with the signatures established by Verhaak and colleagues (2010) (Supplementary Table 6).

Based on the sample data classified as proneural, proliferative or mesenchymal in previous studies, Carro and colleagues defined a subset of transcription factors which function as master regulators of a mesenchymal expression signature, while suppressing a proneural signature in malignant gliomas (Carro *et al.* , 2010, Freije *et al.* , 2004, Nigro *et al.* , 2005, Phillips *et al.* , 2006). Comparison of this comprehensive dataset with the set of genes that were differentially regulated in LNT-229 siTB4 cells revealed an up-regulation of 20 genes of the proneural signature and silencing of 23 proliferative signature genes (Supplementary Table 7). Furthermore, 10 transcription factors that had been predicted by an ARACNe based master regulator algorithm to be frequently connected to the mesenchymal signature, or had consensus enrichment in the promoters of mesenchymal signature genes (Carro *et al.* , 2010), respectively, were down-regulated in LNT-229 siTB4 cells (Fig. 5B). Conversely, the inhibitor of the mesenchymal signature *SATB1* was up-regulated upon TB4 gene silencing (Fig. 5B). These data indicate that TB4 gene silencing inhibits the mesenchymal signature and shifts the balance towards a more differentiated expression pattern. In line with this, a set of 20 genes that are down-regulated during *in vitro* astrocyte development were also down-regulated in LNT-229 siTB4 cells (Supplementary Table 8) (Cahoy *et al.* , 2008).

TB4 gene silencing in GS-2 cells reduces stemness *in vitro* and *in vivo*

The analyses summarized above suggested that TB4 promotes the mesenchymal signature in glioma cells. To further analyze the functional relevance of this finding, we investigated the role of TB4 in the glioma stem-like cell line GS-2 (Gunther *et al.* , 2008). We efficiently depleted TB4 expression in GS-2 cells as assessed by qRT-PCR and immunoblot (Fig. 6A and B). TB4 depletion decreased cellular growth (Fig. 6C) and sphere

formation (Fig. 6D). The sphere volume was reduced in GS-2 siTB4 to 16.12 +/- 1.97 % ($p<0.0001$) (Fig. 6E).

Next, we assessed the differentiation capacity of GS-2 siTB4 versus GS-2 scr cells using increasing FCS concentrations as a stimulus to induce differentiation. FCS treatment yielded a maximum of 5.8 $\pm$ 0.9-fold increase ($p<0.0001$) of cells exhibiting an adherent, differentiated phenotype in GS-2 siTB4 (Fig. 6F). Cells that acquired this phenotype expressed glial fibrillary acidic protein (GFAP), but not nestin. Moreover, there was a reduction of nestin-positve cells in GS-2 siTB4 spheres as compared with GS-2 scr while the number of cells expressing GFAP was increased (Fig. 6G). Representative images of GS-2 scr and siTB4 cells grown as spheres or supplemented with 5% FCS for 7 days are shown in Figure 6H and representative stainings of GS-2 scr and siTB4 cells are outlined in Figure 6I.

Finally, we assessed the tumorigenicity of GS-2 siTB4 cells *in vivo*. Even after implantation of 200.000 cells, we did not observe any neurological symptoms in GS-2 siTB4-glioma-bearing mice until day 140 whereas GS-2 scr-glioma-bearing mice developed neurological symptoms within 69-87 (median 78) days (Fig. 6J). After 140 days, we sacrificed the asymptomatic GS-2 siTB4-glioma-bearing animals and analyzed the brains by histology. Tumor formation had occurred only in 3 of 7 animals (Fig. 7A and B). The expression of nestin was reduced (Fig. 7C and D). Expression of GFAP was similar in both groups (Fig. 7E and F). We did not detect the neural lineage marker NeuN in GS-2 scr gliomas (Fig. 7G) whereas NeuN-positive cells were present in GS-2 siTB4 gliomas (Fig. 7H).

DISCUSSION

TB4 is a key regulator of cancer hallmarks including migration, invasion, cell survival and stem cell activation (Bock-Marquette *et al.* , 2004, Fan *et al.* , 2009, Smart *et al.* , 2007). In neural stem cells, TB4 gene silencing promotes neural differentiation, whereas overexpression of TB4 in the developing brain leads to an expansion of the neuroglial stem and progenitor cell pool and induction of a mesenchymal phenotype (Mollinari *et al.* , 2009, Wirsching *et al.* , 2012). The sub-population of stem-like cells in gliomas termed GIC exhibits features of neuroglial progenitor cells, including self-renewal and multilineage differentiation, and expresses a mesenchymal gene signature (Bao *et al.* , 2006, Carro *et al.* , 2010, Chen *et al.* , 2012, Galli *et al.* , 2004). The role of TB4 during brain development and for mesenchymal transformation prompted us to hypothesize a role of TB4 in malignant glioma.

As a first step to investigate a role for TB4 in malignant glioma, we performed TMA, REMBRANDT and TCGA analyses (Fig. 1, Supplementary Fig. 1). TB4 expression correlated with ascending grades of malignancy and with survival. TMA data suggested that the correlation of TB4 staining intensity with increasing WHO grade was due to an increase of TB4 staining intensity within the tumor cell compartment (Fig. 1, Supplementary Fig. 1). Thus, we focused our further analyses on TB4 in glioma cells.

Both, long-term glioma and GIC lines expressed high levels of TB4 *in vitro* (Supplementary Fig. 2). Silencing of TB4 in long-term glioma cells promoted apoptotic cell death upon nutrient depletion (Fig. 2, Supplementary Fig. 5), inhibited migration and invasion (Fig. 3, Supplementary Fig. 5) and increased survival of glioma-bearing nude mice (Fig. 4). Upon the onset of clinical symptoms, LNT-229 siTB4 gliomas resemble LNT-229 scr gliomas in terms of tumor size and invasiveness, thus suggesting a compensation for TB4 gene silencing in an advanced stages of the disease (Supplementary Fig. 7).

Alterations of the cellular morphology from spindle-like to a more dense and adhesive pattern upon TB4 depletion suggested altered actin dynamics to be the underlying mechanism by which TB4 mediates its cellular functions (Fig. 2). However, enhanced starvation-induced apoptotic cell death pointed to a functional

significance of TB4 beyond its well-established role as an actin-buffering polypeptide (Fan *et al.* , 2009). Thus, we reasoned that alteration of intracellular signaling pathways may contribute to the observed *in vitro* and *in vivo* effects of TB4 gene silencing in glioma. To further elucidate the underlying mechanism of TB4 gene silencing-mediated effects, we first investigated known interactions by which TB4 modulates cellular functions in other cell types. During cardiac development and in migrating endothelial cells TB4 stabilizes ILK, thus promoting Akt phosphorylation and MMP2 expression (Bock-Marquette *et al.* , 2004, Fan *et al.* , 2009). Furthermore, TB4-induced epithelial-mesenchymal transition and malignant progression of colon adenoma to carcinoma is mediated by ILK stabilization and activation (Huang *et al.* , 2007). In turn, TB4 depletion in colon cancer cells leads to reduced ILK activity, reduced tumor volumes and cell migration (Ricci-Vitiani *et al.* , 2010). In LNT-229 glioma cells, ILK protein levels were not reduced upon TB4 gene silencing, unless PI3K signaling was inhibited by wortmannin. However, even strongly decreased ILK protein levels did not affect Akt phosphorylation or MMP2 protein level (Supplementary Fig. 8) suggesting compensatory mechanisms for down-regulation of ILK.

To unravel the molecular network of TB4 in glioma cells, we performed a genome-wide screening for genes that were differentially transcribed upon TB4 gene silencing (Fig. 5). In the past decade, several molecular subgroups of malignant gliomas based on genetic signatures have been defined and correlated to clinical outcome (Phillips *et al.* , 2006, Verhaak *et al.* , 2010). Expression of proneural marker genes correlates with better clinical outcome whereas mesenchymal and proliferative signatures were associated with poor outcome (Carro *et al.* , 2010, Freije *et al.* , 2004, Phillips *et al.* , 2006). Consequently, we compared the TB4-dependently regulated set of genes with the genetic signatures of these previously published molecular subgroups. This comparison revealed regulation of various mesenchymal signature genes in the sense of a shift towards a more differentiated molecular subgroup in siTB4 cells (Fig. 5, Supplementary Tables 6 and 7).

As GIC more closely reflect the functional relevance of a shift towards a more differentiated molecular subgroup than long-term glioma cell lines (Galli *et al.* , 2004, Singh *et al.* , 2004) we analyzed the role of TB4 expression in the GIC line GS-2 (Gunther *et al.* , 2008). TB4 depletion in GS-2 cells inhibited self-renewal,

decreased sphere size and increased differentiation capacity *in vitro* (Fig. 6), and strongly reduced tumorigenicity and increased differentiation capacity *in vivo* (Fig. 7). These data are supported by previous reports suggesting a role of TB4 for stemness during brain and cardiac development (Bock-Marquette *et al.* , 2004, Wirsching *et al.* , 2012).

GS-4 cells share molecular features with GS-2 (Gunther *et al.* , 2008), but, as opposed to GS-2, GS-4 express little if any TB4 (Supplementary Fig. 2). In line with our observations on the role of TB4 for stemness and differentiation, GS-4 cells are not tumorigenic in nude mice, express lower levels of the progenitor marker nestin, higher levels of the differentiation markers MAP2 and BAI1, and exhibit an adherent growth pattern (Gunther *et al.* , 2008).

Functional interactome analysis of the TB4-dependently regulated set of genes using STRING and subsequent cluster analysis revealed a network involving p53 and TGF-β signaling (Fig. 5). Of note, recent studies have demonstrated that TGF-β mediates promotion of stemness in gliomas (Anido *et al.* , 2010), thus suggesting a mechanism by which a siTB4-mediated decrease of TGF-β signaling may have decreased stemness in GS-2 cells (Fig. 6 and 7).

We further confirmed altered TGF-β signaling by data derived from qRT-PCR, ELISA and reporter assays indicating a decreased TGF-β_1 and TGF-β_2 transcription and signaling upon TB4 depletion (Supplementary Fig. 9). One well-established function of TGF-β in gliomas is immunomodulation in the tumor microenvironment (Massague, 2008). Immunomodulation, however, is unlikely to have played a significant role for the prolonged survival in our orthotopic xenograft models, as these experiments were performed in immunodeficient mice (Figs. 4 and 6).

In summary, TB4 expression correlates with glioma grades and patients' survival, and regulates key malignant features in glioma models, including cell survival, invasiveness and stemness. Thereby, TB4 modulates core molecular networks including p53 and TGF-β signaling. We conclude that TB4 might be a novel key molecule integrating multiple hallmarks and molecular networks in malignant gliomas and should thus be further explored as a putative therapeutic target. To date, the only molecular inhibitor known to

interfere with TB4 is *Photorabdus* toxin complex 3, which inhibits the interaction of TB4 with G-actin (Lang *et al.* , 2010), but inhibition of the TB4-actin interaction alone is likely to yield activation of other cancer relevant pathways (Fan *et al.* , 2009). Antisense strategies for targeting gene expression are conceivable, but have had limited success in cancer treatment so far. Recently, a first antisense therapy has been approved by the United States Food and Drug Administration to target apolipoprotein B in familial hypercholesterolemia (Gotto and Moon, 2013). Limitations for such an approach in malignant glioma include tumor heterogeneity and the uncertainty of how efficient down-regulation would have to be to exert activity. Yet, the design of pharmacological inhibitors of TB4 function seems feasible, given innovative high-throughput screening of small molecule libraries (Zhang *et al.* , 2009). Small molecule inhibitors could either target TB4 function directly or its down-stream mediators. Thus, a thorough investigation of molecular interactions in the TB4 network in gliomas is needed.

Acknowledgements

This work was supported by the Deutsche Forschungsgemeinschaft (SFB 773, A6), by the NCCR Neural Plasticity and Repair (P4) and by the Krebsliga Zürich. We thank Caroline Herrmann (Department of Preclinical Imaging and Radiopharmacy, University of Tübingen, Tübingen, Germany, chairman: Bernd Pichler), Silvia Dolski and Matthias Scholl (Laboratory of Molecular Neuro-Oncology, Department of Neurology, University Hospital Zurich, Zurich, Switzerland) for outstanding technical assistance. We also thank René Deenen (Center for Biological and Medical Research, BMFZ, Heinrich Heine University, Düsseldorf) for help with the evaluation of microarray data and Katrin Lamszus (Laboratory for Brain Tumor Biology, Department of Neurosurgery, University Medical Center Hamburg-Eppendorf, Hamburg, Germany) for GS cells.

FIGURE LEGENDS

Fig. 1: TB4 is overexpressed in high-grade gliomas and low TB4 expression correlates with better outcome

A: Representative images of TB4 immunostainings of a TMA comprising 89 gliomas of different WHO grades (II-IV) and 4 normal brain control samples (NB). *B:* x, WHO grade, y, TB4 staining intensity (arbitrary units; *p<0.05, **p<0.01). *C:* TB4 immunoreactivity scores in the tumor cell compartment of WHO grade II-IV patients' samples (***p<0.001). *D:* TB4 immunoreactivity scores in glioblastoma (GBM, WHO grade IV) stratified for tumor cells (TC), endothelial cells (EC) and inflammatory host cells (HC) (***p<0.001). *E:* Survival analysis of patients with glioblastomas (WHO grade IV) subdivided by low (0-2) versus high (>2) TB4 staining intensity. *F:* REMBRANDT survival analysis of patients with glioblastoma subdivided by low (<0.5-fold, green, n=6) versus high (>2.0-fold, blue, n=14) TB4 mRNA expression. As a reference, all glioblastoma samples are depicted in grey (n=182). *G:* Immunocytology of LNT-229 glioma cells stained for TB4 (green). Nuclei were stained with DAPI (blue). Scale bars: 100 µm (A), 10 µm (E).

Fig. 2: TB4 gene silencing promotes starvation-induced apoptotic cell death of LNT-229 and U87MG glioma cells

A and B: Quantitative RT-PCR (A) and immunoblot (B) analysis of lentiviral TB4 gene silencing (si) relative to scrambled control shRNA (scr). *C-F:* 10,000 cells per well were seeded in 6-well plates overnight and cultured in serum-free medium for 7 days. *C:* LNT-229 scr and si cells were counted manually using trypan blue for identification of dead cells. Values are expressed as percent of total scr (mean +/- SEM; **p<0.01, ***p<0.001, ****p<0.0001). *D and E:* Propidium iodide (PI) based flow cytometric cell cycle analysis of LNT-229 scr (D) and si (E) cells. *F:* LNT-229 and U87MG scr and si cells were stained with annexinV and PI for identification of life (double negative), dead (PI^+) and apoptotic ($annexinV^+$) cell fractions. *G-L:* LNT-

229 scr and si cells were studied by colony formation assay (G and J), for single colony morphology (H and K) and FITC-phalloidin staining of actin filaments (I and L). Arrowheads in I and L indicate cellular protrusions. Scale bars: 1 cm (G and J), 100 µm (H and K) and 25 µm (I and L).

Fig. 3: TB4 gene silencing inhibits invasion of LNT-229 and U87MG glioma cells

*A-L:*Lentivirally transduced LNT-229 or U87MG cells expressing shRNAs targeted against TB4 (si) or a scrambled control (scr) were placed in a three-dimensional collagen I matrix (A-D) and evaluated after 24 h (E-H) and 48 h (I-L); scale bar: 200 µm. *M and N:* The area covered by invading cells (M), or the median distance invaded by the 50 most peripheral cells (N) were measured for quantitation after 48 h (mean +/- SEM; ***p<0.001, ****p<0.0001).

Fig. 4: TB4 gene silencing delays the onset of neurological symptoms and slows tumor growth in orthotopic glioma models

A and B: 7.5 x 10^4 LNT-229 (A) or 10^5 U87MG glioma cells were implanted in the striata of $CD1^{nu/nu}$ mice. Cells were transduced with a lentivirus coding for shRNA targeted against TB4 mRNA (si), or a scrambled control sequence (scr). Animals (n=7 per group) were sacrificed upon onset of neurological symptoms. *C:* H&E staining of LNT-229 tumors from animals (n=3 per group) sacrificed on day 28 post implantation for histological analysis. Scale bar: 200 µm.

Fig. 5: The differentially regulated transcriptional network in TB4-depleted glioma cells involves master regulators of mesenchymal transition

A: Transcription factors that were differentially regulated in LNT-229 glioma cells after lentiviral TB4 gene silencing were determined by Affymetrix gene chip analysis. Functional interactions were analyzed using the Search Tool for the Retrieval of Interacting Genes/Proteins (STRING). Interactions with confidence scores of 0.9 or higher were integrated to the depicted interactome. Clusters were determined by the MCL algorithm at low inflation and are represented by different node colors (green, red, brown, yellow and blue). Inter-cluster edges are represented by dashed-lines. *B:* Master molecules of the transcriptional network that promotes mesenchymal transformation of malignant gliomas were assessed by master regulator analysis (MRA) and regulon analysis (DNA binding) (Carro *et al.* , 2010). Depicted are those genes that were at least 2-fold upregulated (red) or downregulated (green) after TB4 depletion in LNT-229 cells, as assessed by transcriptome analysis. Asterisk: Inhibitor of the mesenchymal signature.

Fig. 6: TB4 gene silencing in GS-2 cells inhibits self-renewal, promotes differentiation and improves symptom-free survival *in vivo*

A and B: Quantitative RT-PCR (A) and immunoblot (B) analysis of lentiviral TB4 gene silencing (si) relative to scrambled control shRNA (scr) in GS-2 neurosphere cultures. *C:* Acute growth assay. 5,000 GS-2 scr or si cells were seeded in 24-well plates and counted at indicated time points by trypan blue exclusion. *D and E:* Neurosphere formation assay. GS-2 scr or si cells were seeded at single cell dilution (1 cell / 4 µl). Sphere numbers (D) and volume (E) were assessed on day 21. *F:* Differentiation of GS-2 scr or si cells was induced by the addition of FCS at indicated concentrations. Cells exhibiting an adherent phenotype were quantified after 5 days. *G:* Immunocytology was performed in spheres using antibodies for nestin and GFAP. Positive cells were counted in at least 10 high power fields. *H and I:* Representative images of D-F (H), and G (I). *J:* 2 x 10^5 GS-2 scr or si cells were implanted in the striata of $CD1^{nu/nu}$ mice (n=7 for each group). Animals bearing GS-2 scr gliomas were sacrificed upon onset of clinical symptoms. GS-2 si glioma-bearing mice did not

develop symptoms until day 140 (error bars: SEM; Scale bars: 100 µm (H), 50 µm (I); *p<0.05, **p<0.01, ****p<0.0001).

Fig. 7: Histological analysis of GS-2 experimental gliomas

H&E staining (A and B) and immunohistochemistry using antibodies for nestin (C and D), GFAP (E and F) and NeuN (G and H). Asterisks in A indicate hemorrhage. Arrowheads in A and B indicate tumor margins. Scale bars: H&E, 200 µm (A and B), 50 µm (C-H).

Supplementary Fig. 1: Tissue microarray (TMA), REMBRANDT and TCGA data base interrogations

A, Glioblastoma sample, arrowheads in A depict representative tumor cells scored as TB4 high (black) and endothelial cells scored as TB4 low (white). Scale bars: 50 µm. B, Another glioblastoma sample, TB4 or GFAP staining as indicated in the left corner. TB4 is high in the tumor compartment and low in the endothelial compartment. Scale bar 100 µm. *C and D:* TB4 immunoreactivity scores in WHO grade II-IV patients' samples stratified for indicated cell types. *E:* TB4 immunoreactivity scores in glioblastoma stratified for patient age at diagnosis (cutoff: 65 years). *F:* TB4 immunoreactivity scores in primary vs recurrent glioblastoma samples (p<0.05). *G:* REMBRANDT interrogation for TB4 gene expression in WHO grade II-IV patients' samples, expressed as median mRNA expression intensity. *H:* TCGA survival analysis of patients with glioblastoma subdivided by low (n=433) versus high (n=35) TB4 mRNA expression.

Supplementary Fig. 2: TB4 mRNA expression in glioma cell lines and in GIC.

Normal brain control (white bars), long-term glioma cell lines (black bars) and glioma initiating cell lines (grey bars). qRT-PCR was performed using Arf1 as a control gene. Values are expressed as $2^{-\Delta CT}$ (error bars: SEM).

Supplementary Fig. 3: Lentiviral transduction efficacy.

U87MG glioma cells were transduced with lentivirus expressing scrambled control shRNA (scr, A and B), or shRNA for TB4 gene silencing (si, C and D). Transduction efficacy was assessed by dsRed co-expression. Pictures were acquired in bright field (A and C) and red fluorescence (B and D). Scale bar: 100 µm.

Supplementary Fig. 4: TB4 regulates cellular growth and metabolism in glioma cells

A: qRT-PCR confirmation of lentiviral TB4 overexpression (TB4) as compared to empty vector controls (Ctr) in LNT-229 and U87MG glioma cells. *B and C:* 5,000 LNT-229 glioma cells were seeded per well in 24-well plates and counted daily by trypan blue exclusion. Cells were transduced with lentivirus for Ctr or TB4 (B), or for expression of shRNA targeting TB4 (si) or a scrambled control sequence (scr, C). *D:* 1,000 LNT-229 si and scr transduced cells per well were seeded in 96-well plates and Alamar blue metabolism assay was performed at indicated time points.

Supplementary Fig. 5: TB4 gene silencing using a second shRNA target sequence confirms increased cell death upon serum starvation and decreased invasion

A: qRT-PCR confirmation of lentiviral TB4 gene silencing (si_2) as compared to a scrambled control shRNA (scr; mean +/- SEM). *B-D:* 10,000 cells per well were seeded in 6-well plates overnight and cultured in serum-free medium for 7 days. *B and C:* Representative images on day 7; scale bar: 200 µm. *D:* LNT-229 scr and si_2 cells were counted manually using trypan blue for identification of dead cells. Values are expressed as percent of total scr (mean +/- SEM; ***p<0.001, ****p<0.0001). *E-J:*Lentivirally transduced LNT-229 scr or si_2 cells were placed in a three-dimensional collagen I matrix (E and F) and evaluated after 24 h (G and

H) and 48 h (I and J); scale bar in J: 200 µm. *K and L:* The area covered by invading cells (K), or the median distance invaded by the 50 most peripheral cells (L) were measured for quantitation after 48 h (mean +/- SEM; ***p<0.001, ****p<0.0001).

Supplementary Fig. 6: TB4 gene silencing decreases migration of glioma cells

50,000 cells per well were seeded in the upper wells of a 24-well transwell migration assay. LNT-229 and U87MG glioma cells were transduced with lentivirus for TB4 overexpression (TB4) or gene silencing (si), or with respective control viruses (Ctr, scr). Cells were allowed to migrate for 16 h (*p<0.05, **p<0.01, ****p<0.0001).

Supplementary Fig. 7: Histological analysis of LNT-229 experimental gliomas at the timepoint of clinical tumor progression

H&E stainings of representative tumors were analysed upon development of clinical symptoms. LNT-229 glioma cells were transduced with lentivirus expressing scrambled control shRNA (scr, A), or shRNA for TB4 gene silencing (si, B). Scale bar: 200 µm.

Supplementary Fig. 8: TB4 gene silencing reduces MMP activity

A: Lentivirally TB4-depleted (si) or scrambled control (scr) LNT-229 cells were cultured with or without wortmannin (WM) for 24 h. Immunoblot was performed using antibodies for ILK, Akt, β-Actin or phospho-specific antibody to Akt-Ser473 (pAkt). *B:* Immunoblot of LNT-229 scr and si cells using antibodies for MMP2 and β-Actin. *C:* FRET-based MMP-activity assay (*p<0.05).

Supplementary Fig. 9: Inhibition of TGF-β signaling upon TB4 gene silencing

A and B: qRT-PCR of lentivirally TB4-depleted (si) or scrambled control (scr) LNT-229 or U87MG cDNAs was performed using primers for *TGFB1* (A) and *TGFB2* (B). *C and D:* ELISA of LNT-229 scr and si conditioned media was performed using antibodies against TGF-β_1 (C) and TGF-β_2 (D). *E:* Dual luciferase/renilla TGF-β signaling reporter assay. LNT-229 scr and si cells were co-transfected with pRL-CMV and either the Smad-binding element containing pGL3-SBE2-Luc (pSBE2), or the plasminogen activator inhibitor 1 (PAI-1) promoter containing pGL2-3TP-Luc (3TP) (scale bar: 200 μm; *p<0.05, **p<0.01).

Supplementary video: Time-lapse recording of invading U87MG scr & U87MG siTB4 cells

Supplementary Table 1 Scoring system for the assessment of clinical tumor progression.

Supplementary Table 2: Clinical data and TB4 expression levels of tissue microarray patients' samples.

Hist: Sample histological diagnosis; *Age*: Age at diagnosis; *Loc*: Tumor localization; *Res*: Extent of resection; *RTx*: Radiotherapy; *TMZ*: Chemotherapy with Temozolomide; *Other*: Other systemic therapy; *TB4*: Thymosin beta4 expression levels (arbitrary units); *Surv*: Survival in months; *A*: Astrocytoma, not specified; *FA*: Fibrillary Astrocytoma; *OD*: Oligodendroglioma; *OA*: Oligoastrocytoma; *XA*: Pleomorphic Xanthoastrocytoma; *AA*: Anaplastic Astrocytoma; *AO*: Anaplastic Oligodendroglioma; *AOA*: Anaplastic Oligoastrocytoma; *GA*: Gemistocytic Astrocytoma; *GBM*: Glioblastoma, primary diagnoses of secondary GBMs are depicted in braces; *GSR*: Gliosarcoma; *l*: Left hemisphere; *r*: Right hemisphere; *frt*: Frontal lobe;

prt: Parietal lobe; *tmp*: Temporal lobe; *occ*: Occipital lobe; *ins*: Insula; *hpc*: Hippocampus; *cng*: Gyrus cinguli; *tha*: Thalamus; *bs*: Brain stem; *CCNU*: Lomustin; *BEV*: Bevacizumab; *IRI*: Irinotecan; *GEF*: Gefitinib; *THL*: Thalidomide.

Supplementary Table 3 Affymetrix total mRNA expression analysis was performed in LNT-229 cells after TB4 gene silencing. All transcription factors and corresponding probe sets that are up-regulated (red) or down-regulated (green) by at least 2-fold are listed hierarchically.

Supplementary Table 4 Affymetrix total mRNA expression analysis was performed in LNT-229 cells after TB4 gene silencing. Genes and corresponding probe sets annotated to migration by gene ontology are listed hierarchically.

Supplementary Table 5 Affymetrix total mRNA expression analysis was performed in LNT-229 cells after TB4 gene silencing. Genes and corresponding probe sets annotated to apoptosis by gene ontology are listed hierarchically.

Supplementary Table 6 Affymetrix total mRNA expression analysis was performed in LNT-229 siTB4 cells. Differentially regulated genes were compared to the glioma signatures of up- and down-regulated genes defined by centroid-based clustering by Verhaak and colleagues (Verhaak *et al.* , 2010). Up-regulation (red) or gene silencing (green) by at least 2-fold in LNT-229 siTB4 is depicted by color as indicated.

Supplementary Table 7 Affymetrix total mRNA expression analysis was performed in LNT-229 siTB4 cells. Differentially regulated genes were compared to the glioma gene signatures defined by Carro and colleagues (Carro *et al.* , 2010). Up-regulation (red) or gene silencing (green) by at least 2-fold in LNT-229 siTB4 is depicted by color as indicated.

Supplementary Table 8 Affymetrix total mRNA expression analysis was performed in LNT-229 siTB4 cells. Differentially regulated genes were compared to the genes up- or down-regulated during astrocyte or oligodendrocyte development (Cahoy *et al.* , 2008). Up-regulation (red) or gene silencing (green) by at least 2-fold in LNT-229 siTB4 is depicted by color as indicated.

REFERENCES

Albini A, Iwamoto Y, Kleinman HK, Martin GR, Aaronson SA, Kozlowski JM, et al. A rapid in vitro assay for quantitating the invasive potential of tumor cells. Cancer Res. 1987 Jun 15;47(12):3239-45.

Anido J, Saez-Borderias A, Gonzalez-Junca A, Rodon L, Folch G, Carmona MA, et al. TGF-beta Receptor Inhibitors Target the CD44(high)/Id1(high) Glioma-Initiating Cell Population in Human Glioblastoma. Cancer Cell. 2010 Dec 14;18(6):655-68.

Bahr O, Rieger J, Duffner F, Meyermann R, Weller M, Wick W. P-glycoprotein and multidrug resistance-associated protein mediate specific patterns of multidrug resistance in malignant glioma cell lines, but not in primary glioma cells. Brain Pathol. 2003 Oct;13(4):482-94.

Bao S, Wu Q, McLendon RE, Hao Y, Shi Q, Hjelmeland AB, et al. Glioma stem cells promote radioresistance by preferential activation of the DNA damage response. Nature. 2006 Dec 7;444(7120):756-60.

Bock-Marquette I, Saxena A, White MD, Dimaio JM, Srivastava D. Thymosin beta4 activates integrin-linked kinase and promotes cardiac cell migration, survival and cardiac repair. Nature. 2004 Nov 25;432(7016):466-72.

Cahoy JD, Emery B, Kaushal A, Foo LC, Zamanian JL, Christopherson KS, et al. A transcriptome database for astrocytes, neurons, and oligodendrocytes: a new resource for understanding brain development and function. J Neurosci. 2008 Jan 2;28(1):264-78.

Carro MS, Lim WK, Alvarez MJ, Bollo RJ, Zhao X, Snyder EY, et al. The transcriptional network for mesenchymal transformation of brain tumours. Nature. 2010 Jan 21;463(7279):318-25.

Chen J, Li Y, Yu TS, McKay RM, Burns DK, Kernie SG, et al. A restricted cell population propagates glioblastoma growth after chemotherapy. Nature. 2012 Aug 23;488(7412):522-6.

Demaison C, Parsley K, Brouns G, Scherr M, Battmer K, Kinnon C, et al. High-level transduction and gene expression in hematopoietic repopulating cells using a human immunodeficiency

[correction of imunodeficiency] virus type 1-based lentiviral vector containing an internal spleen focus forming virus promoter. Hum Gene Ther. 2002 May 1;13(7):803-13.

Fan Y, Gong Y, Ghosh PK, Graham LM, Fox PL. Spatial coordination of actin polymerization and ILK-Akt2 activity during endothelial cell migration. Dev Cell. 2009 May;16(5):661-74.

Freije WA, Castro-Vargas FE, Fang Z, Horvath S, Cloughesy T, Liau LM, et al. Gene expression profiling of gliomas strongly predicts survival. Cancer Res. 2004 Sep 15;64(18):6503-10.

Galli R, Binda E, Orfanelli U, Cipelletti B, Gritti A, De Vitis S, et al. Isolation and characterization of tumorigenic, stem-like neural precursors from human glioblastoma. Cancer Res. 2004 Oct 1;64(19):7011-21.

Gilbert MR, Wang M, Aldape KD, Stupp R, Hegi M, Jaeckle KA, et al. RTOG 0525: A randomized phase III trial comparing standard adjuvant temozolomide (TMZ) with a dose-dense (dd) schedule in newly diagnosed glioblastoma (GBM). ASCO Meeting Abstracts. 2011 June 9, 2011;29(15_suppl):2006.

Gotto AM, Jr., Moon JE. Pharmacotherapies for lipid modification: beyond the statins. Nat Rev Cardiol. 2013 Aug 20.

Gunther HS, Schmidt NO, Phillips HS, Kemming D, Kharbanda S, Soriano R, et al. Glioblastoma-derived stem cell-enriched cultures form distinct subgroups according to molecular and phenotypic criteria. Oncogene. 2008 May 1;27(20):2897-909.

Hanahan D, Weinberg RA. Hallmarks of cancer: the next generation. Cell. 2011 Mar 4;144(5):646-74.

Huang HC, Hu CH, Tang MC, Wang WS, Chen PM, Su Y. Thymosin beta4 triggers an epithelial-mesenchymal transition in colorectal carcinoma by upregulating integrin-linked kinase. Oncogene. 2007 Apr 26;26(19):2781-90.

Ikushima H, Todo T, Ino Y, Takahashi M, Miyazawa K, Miyazono K. Autocrine TGF-beta signaling maintains tumorigenicity of glioma-initiating cells through Sry-related HMG-box factors. Cell Stem Cell. 2009 Nov 6;5(5):504-14.

Johnson DR, O'Neill BP. Glioblastoma survival in the United States before and during the temozolomide era. J Neurooncol. 2012 Apr;107(2):359-64.

Kim Y, Kim EH, Hong S, Rhyu IJ, Choe J, Sun W, et al. Expression of thymosin beta in the rat brain following transient global ischemia. Brain Res. 2006 Apr 26;1085(1):177-82.

Lang AE, Schmidt G, Schlosser A, Hey TD, Larrinua IM, Sheets JJ, et al. Photorhabdus luminescens toxins ADP-ribosylate actin and RhoA to force actin clustering. Science. 2010 Feb 26;327(5969):1139-42.

Liu HK, Wang Y, Belz T, Bock D, Takacs A, Radlwimmer B, et al. The nuclear receptor tailless induces long-term neural stem cell expansion and brain tumor initiation. Genes Dev. 2010 Apr 1;24(7):683-95.

Low TL, Thurman GB, McAdoo M, McClure J, Rossio JL, Naylor PH, et al. The chemistry and biology of thymosin. I. Isolation, characterization, and biological activities of thymosin alpha1 and polypeptide beta1 from calf thymus. J Biol Chem. 1979 Feb 10;254(3):981-6.

Massague J. TGFbeta in Cancer. Cell. 2008 Jul 25;134(2):215-30.

McLendon R, Friedman A, Bigner D, Van Meir E, Brat D, Mastrogianakis G, et al. Comprehensive genomic characterization defines human glioblastoma genes and core pathways. Nature. 2008 Oct 23;455(7216):1061-8.

Mohring T, Kellmann M, Jurgens M, Schrader M. Top-down identification of endogenous peptides up to 9 kDa in cerebrospinal fluid and brain tissue by nanoelectrospray quadrupole time-of-flight tandem mass spectrometry. J Mass Spectrom. 2005 Feb;40(2):214-26.

Mollinari C, Ricci-Vitiani L, Pieri M, Lucantoni C, Rinaldi AM, Racaniello M, et al. Downregulation of thymosin beta4 in neural progenitor grafts promotes spinal cord regeneration. J Cell Sci. 2009 Nov 15;122(Pt 22):4195-207.

NCI. REMBRANDT homepage. http://rembrandtncinihgov. 2005.

Nigro JM, Misra A, Zhang L, Smirnov I, Colman H, Griffin C, et al. Integrated array-comparative genomic hybridization and expression array profiles identify clinically relevant molecular subtypes of glioblastoma. Cancer Res. 2005 Mar 1;65(5):1678-86.

Phillips HS, Kharbanda S, Chen R, Forrest WF, Soriano RH, Wu TD, et al. Molecular subclasses of high-grade glioma predict prognosis, delineate a pattern of disease progression, and resemble stages in neurogenesis. Cancer Cell. 2006 Mar;9(3):157-73.

Qian L, Huang Y, Spencer CI, Foley A, Vedantham V, Liu L, et al. In vivo reprogramming of murine cardiac fibroblasts into induced cardiomyocytes. Nature. 2012 May 31;485(7400):593-8.

Ricci-Vitiani L, Mollinari C, di Martino S, Biffoni M, Pilozzi E, Pagliuca A, et al. Thymosin beta4 targeting impairs tumorigenic activity of colon cancer stem cells. FASEB J. 2010 Nov;24(11):4291-301.

Roth LW, Bormann P, Bonnet A, Reinhard E. beta-thymosin is required for axonal tract formation in developing zebrafish brain. Development. 1999 Apr;126(7):1365-74.

Safer D, Golla R, Nachmias VT. Isolation of a 5-kilodalton actin-sequestering peptide from human blood platelets. Proc Natl Acad Sci U S A. 1990 Apr;87(7):2536-40.

Singh SK, Hawkins C, Clarke ID, Squire JA, Bayani J, Hide T, et al. Identification of human brain tumour initiating cells. Nature. 2004 Nov 18;432(7015):396-401.

Smart N, Risebro CA, Melville AA, Moses K, Schwartz RJ, Chien KR, et al. Thymosin beta4 induces adult epicardial progenitor mobilization and neovascularization. Nature. 2007 Jan 11;445(7124):177-82.

Stupp R, Mason WP, van den Bent MJ, Weller M, Fisher B, Taphoorn MJ, et al. Radiotherapy plus concomitant and adjuvant temozolomide for glioblastoma. N Engl J Med. 2005 Mar 10;352(10):987-96.

Szklarczyk D, Franceschini A, Kuhn M, Simonovic M, Roth A, Minguez P, et al. The STRING database in 2011: functional interaction networks of proteins, globally integrated and scored. Nucleic Acids Res. 2011 Jan;39(Database issue):D561-8.

Tabatabai G, Frank B, Wick A, Lemke D, von Kurthy G, Obermuller U, et al. Synergistic antiglioma activity of radiotherapy and enzastaurin. Ann Neurol. 2007 Feb;61(2):153-61.

Tabatabai G, Hasenbach K, Herrmann C, Maurer G, Mohle R, Marini P, et al. Glioma tropism of lentivirally transduced hematopoietic progenitor cells. Int J Oncol. 2010 Jun;36(6):1409-17.

Vartiainen N, Pyykonen I, Hokfelt T, Koistinaho J. Induction of thymosin beta(4) mRNA following focal brain ischemia. Neuroreport. 1996 Jul 8;7(10):1613-6.

Verhaak RG, Hoadley KA, Purdom E, Wang V, Qi Y, Wilkerson MD, et al. Integrated genomic analysis identifies clinically relevant subtypes of glioblastoma characterized by abnormalities in PDGFRA, IDH1, EGFR, and NF1. Cancer Cell. 2010 Jan 19;17(1):98-110.

Wirsching HG, Kretz O, Morosan-Puopolo G, Chernogorova P, Theiss C, Brand-Saberi B. Thymosin beta4 induces folding of the developing optic tectum in the chicken (Gallus domesticus). J Comp Neurol. 2012 Jun 1;520(8):1650-62.

Wrana JL, Attisano L, Carcamo J, Zentella A, Doody J, Laiho M, et al. TGF beta signals through a heteromeric protein kinase receptor complex. Cell. 1992 Dec 11;71(6):1003-14.

Zawel L, Dai JL, Buckhaults P, Zhou S, Kinzler KW, Vogelstein B, et al. Human Smad3 and Smad4 are sequence-specific transcription activators. Mol Cell. 1998 Mar;1(4):611-7.

Zhang J, Yang PL, Gray NS. Targeting cancer with small molecule kinase inhibitors. Nat Rev Cancer. 2009 Jan;9(1):28-39.

Zheng H, Ying H, Yan H, Kimmelman AC, Hiller DJ, Chen AJ, et al. p53 and Pten control neural and glioma stem/progenitor cell renewal and differentiation. Nature. 2008 Oct 23;455(7216):1129-33.

Figure 1

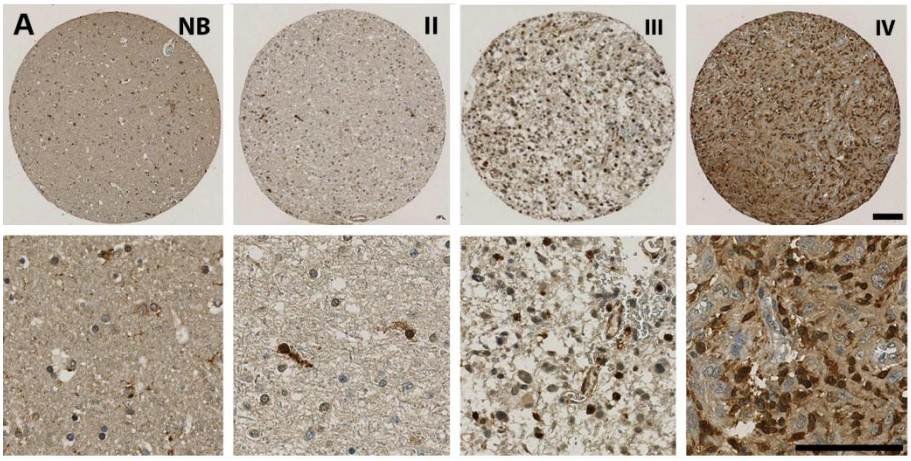
A
NB
II
III
IV

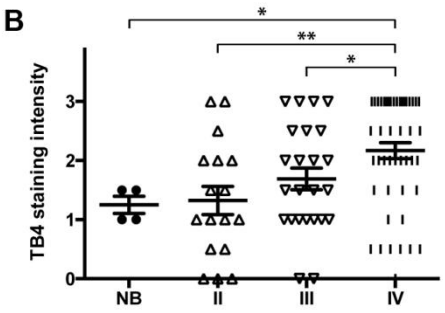
B
TB4 staining intensity
NB
II
III
IV
*
**
*

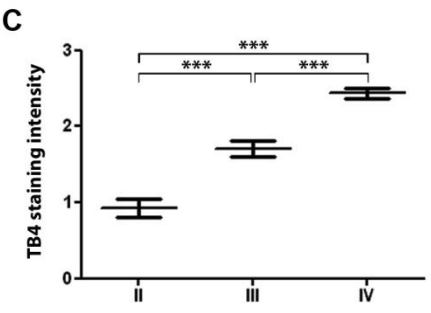
C
TB4 staining intensity
II
III
IV
***
***
***

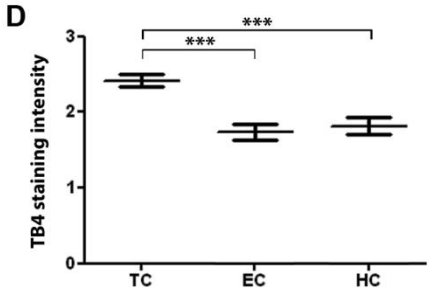
D
TB4 staining intensity
TC
EC
HC
***
***

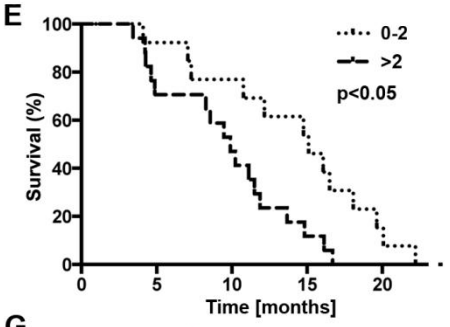
E
Survival (%)
Time [months]
0-2
>2
p<0.05

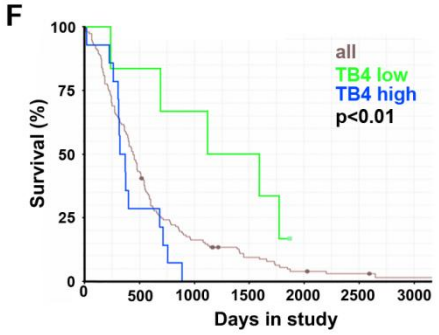
F
Survival (%)
Days in study
all
TB4 low
TB4 high
p<0.01

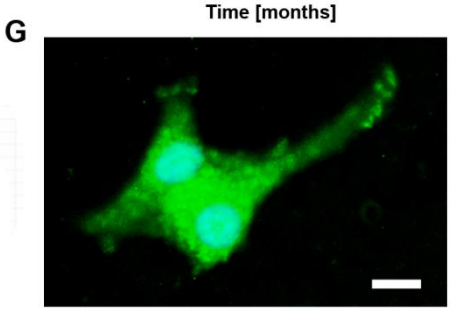
G

Figure 2

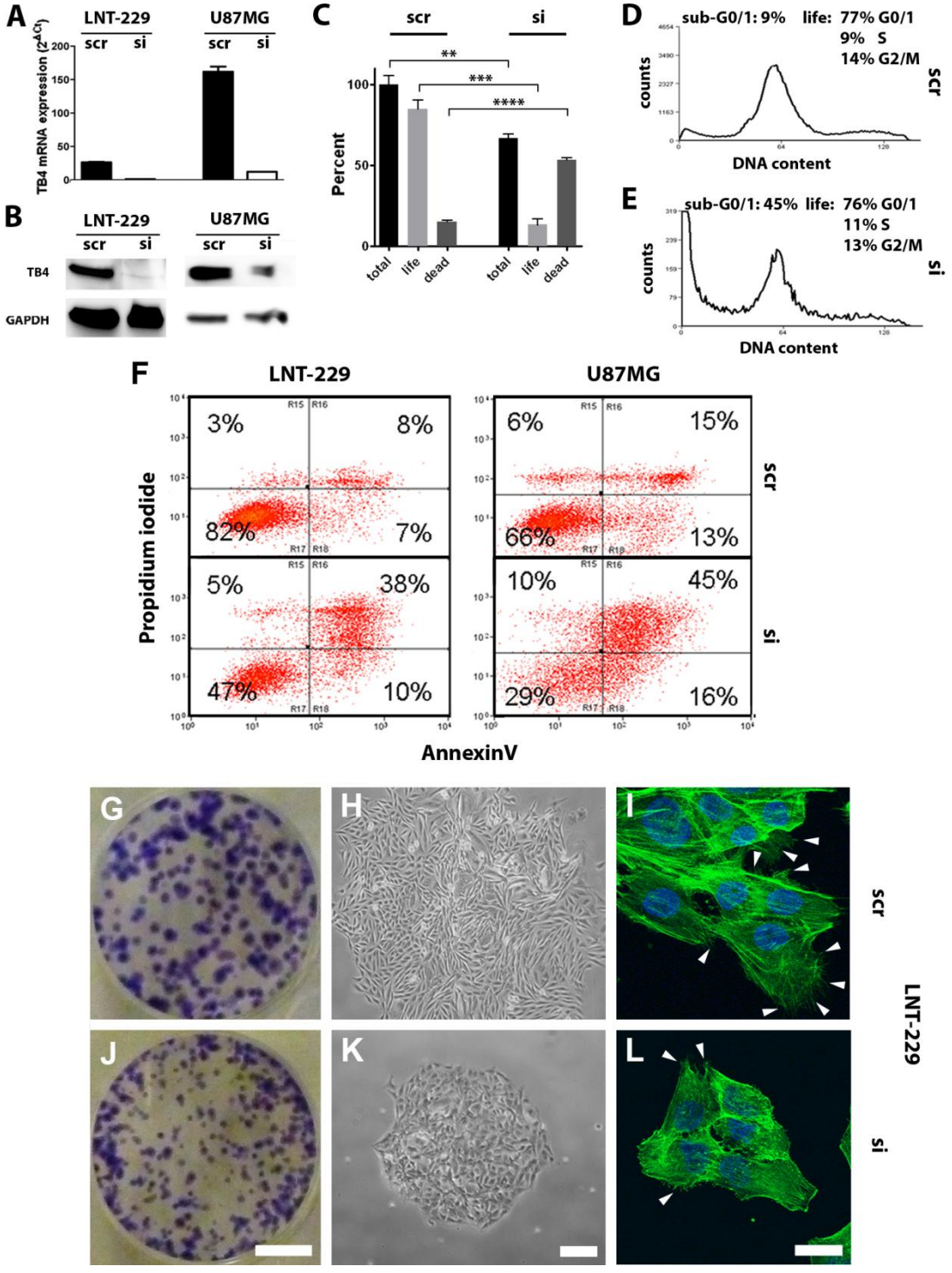
A
LNT-229
U87MG
scr
si
TB4 mRNA expression (2^ΔCt)
B
TB4
GAPDH
C
scr
si
**
***
****
Percent
total
life
dead
D
sub-G0/1: 9%
life: 77% G0/1
9% S
14% G2/M
counts
DNA content
E
sub-G0/1: 45%
life: 76% G0/1
11% S
13% G2/M
F
Propidium iodide
AnnexinV
3%
8%
82%
7%
5%
38%
47%
10%
6%
15%
66%
13%
10%
45%
29%
16%
G
H
I
J
K
L
LNT-229

Figure 3

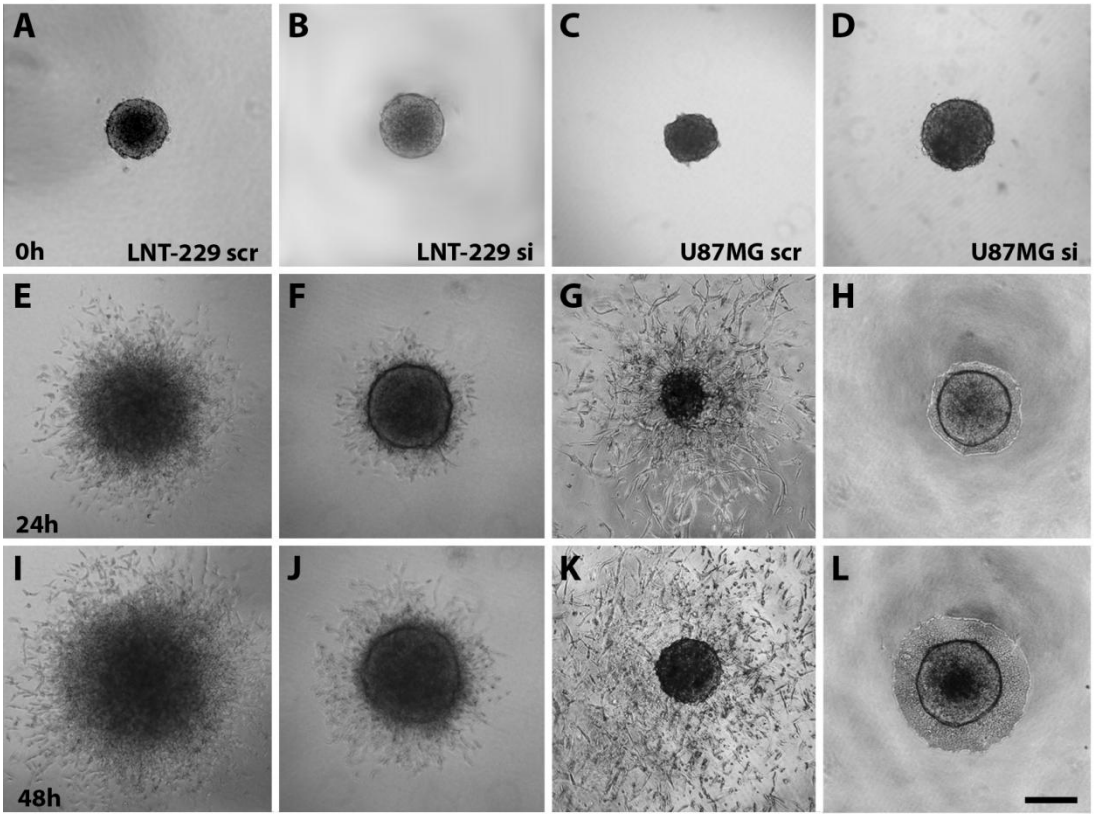
A
B
C
D
0h
LNT-229 scr
LNT-229 si
U87MG scr
U87MG si
E
F
G
H
24h
I
J
K
L
48h
M
Area in µm²
6000
4000
2000
0
***
***
scr
si
scr
si
LNT-229
U87MG
N
Distance in µm
600
400
200
0
****
***
scr
si
scr
si
LNT-229
U87MG

Figure 4

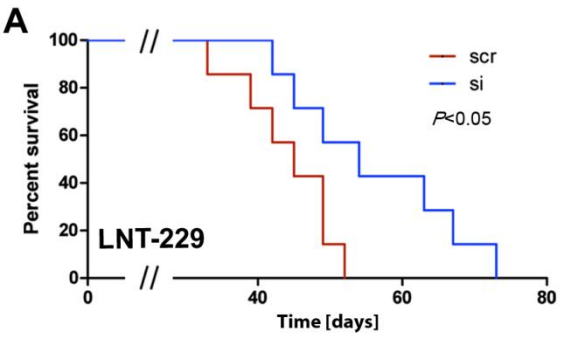
A
100
80
60
40
20
0
Percent survival
//
scr
si
P<0.05
LNT-229
0
40
60
80
Time [days]

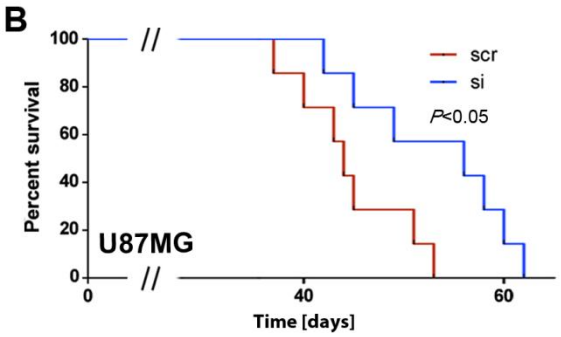
B
100
80
60
40
20
0
Percent survival
//
scr
si
P<0.05
U87MG
0
40
60
Time [days]

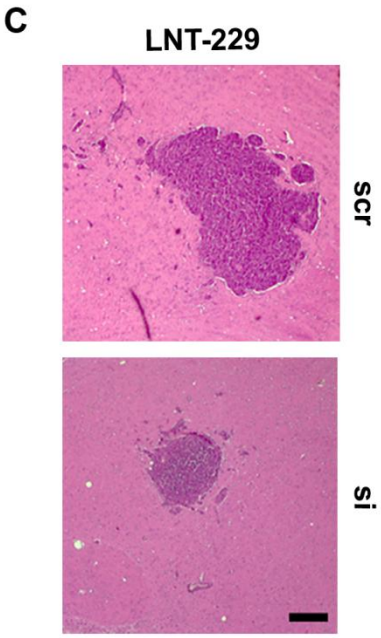
C
LNT-229
scr
si

Figure 5

A

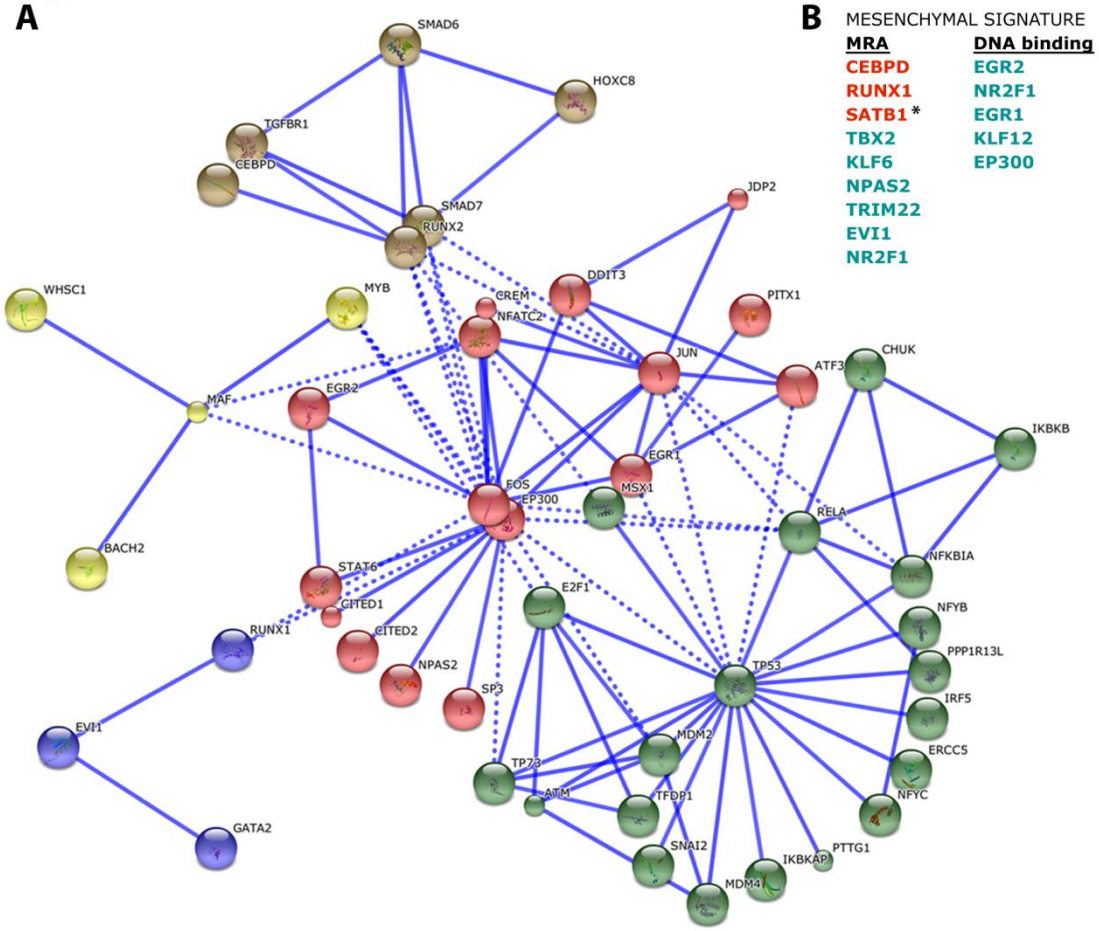

B MESENCHYMAL SIGNATURE

MRA	DNA binding
CEBPD	EGR2
RUNX1	NR2F1
SATB1 *	EGR1
TBX2	KLF12
KLF6	EP300
NPAS2	
TRIM22	
EVI1	
NR2F1	

Figure 6

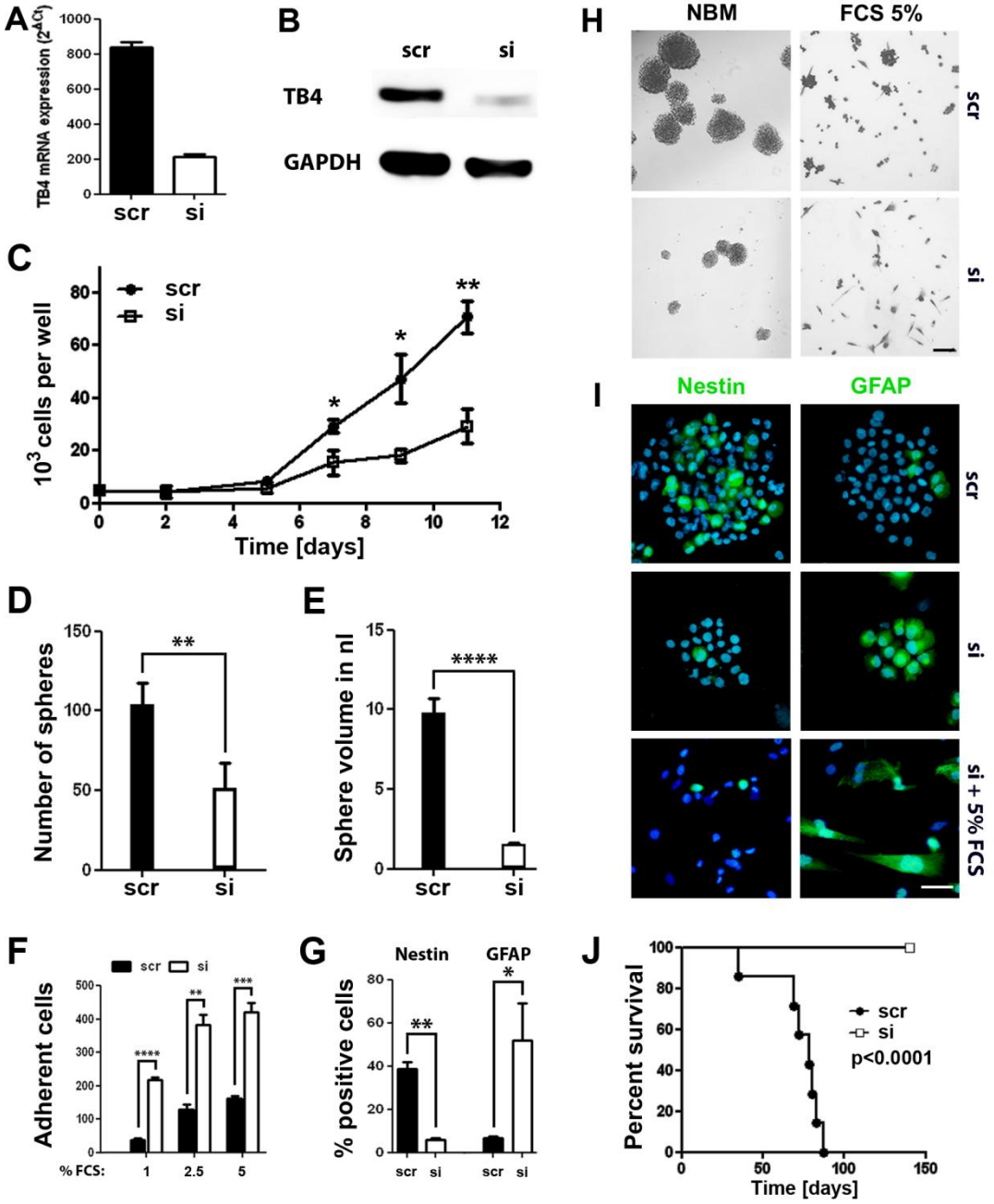
A
TB4 mRNA expression (2^ΔCt)
1000
800
600
400
200
0
scr
si
B
scr
si
TB4
GAPDH
C
scr
si
10^3 cells per well
80
60
40
20
0
0
2
4
6
8
10
12
Time [days]
*
*
**
D
Number of spheres
150
100
50
0
**
scr
si
E
Sphere volume in nl
15
10
5
0
****
scr
si
F
scr
si
Adherent cells
500
400
300
200
100
0
****
**
***
% FCS:
1
2.5
5
G
Nestin
GFAP
% positive cells
80
60
40
20
0
**
*
scr
si
scr
si
H
NBM
FCS 5%
scr
si
I
Nestin
GFAP
scr
si
si + 5% FCS
J
Percent survival
100
80
60
40
20
0
0
50
100
150
Time [days]
scr
si
p<0.0001

Figure 7

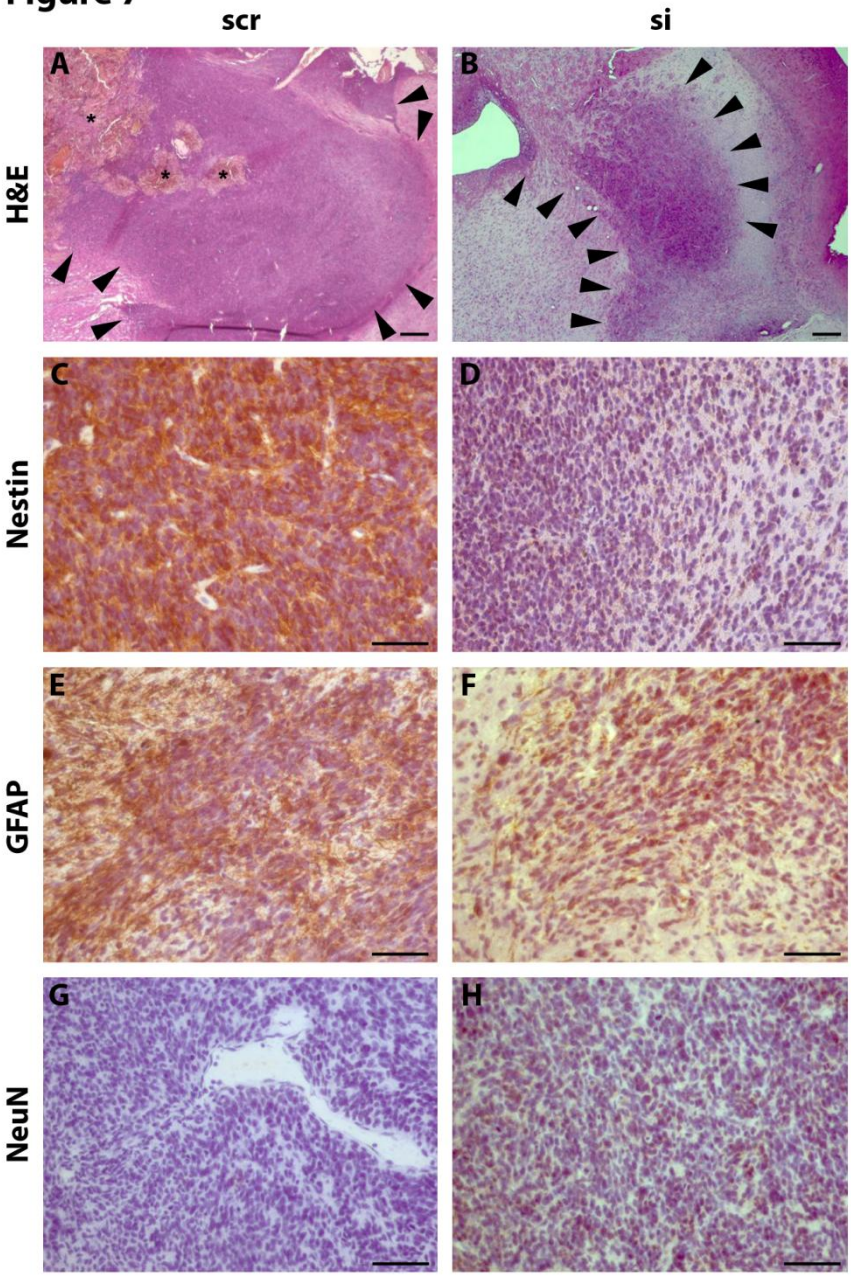

Supplementary Figure 1

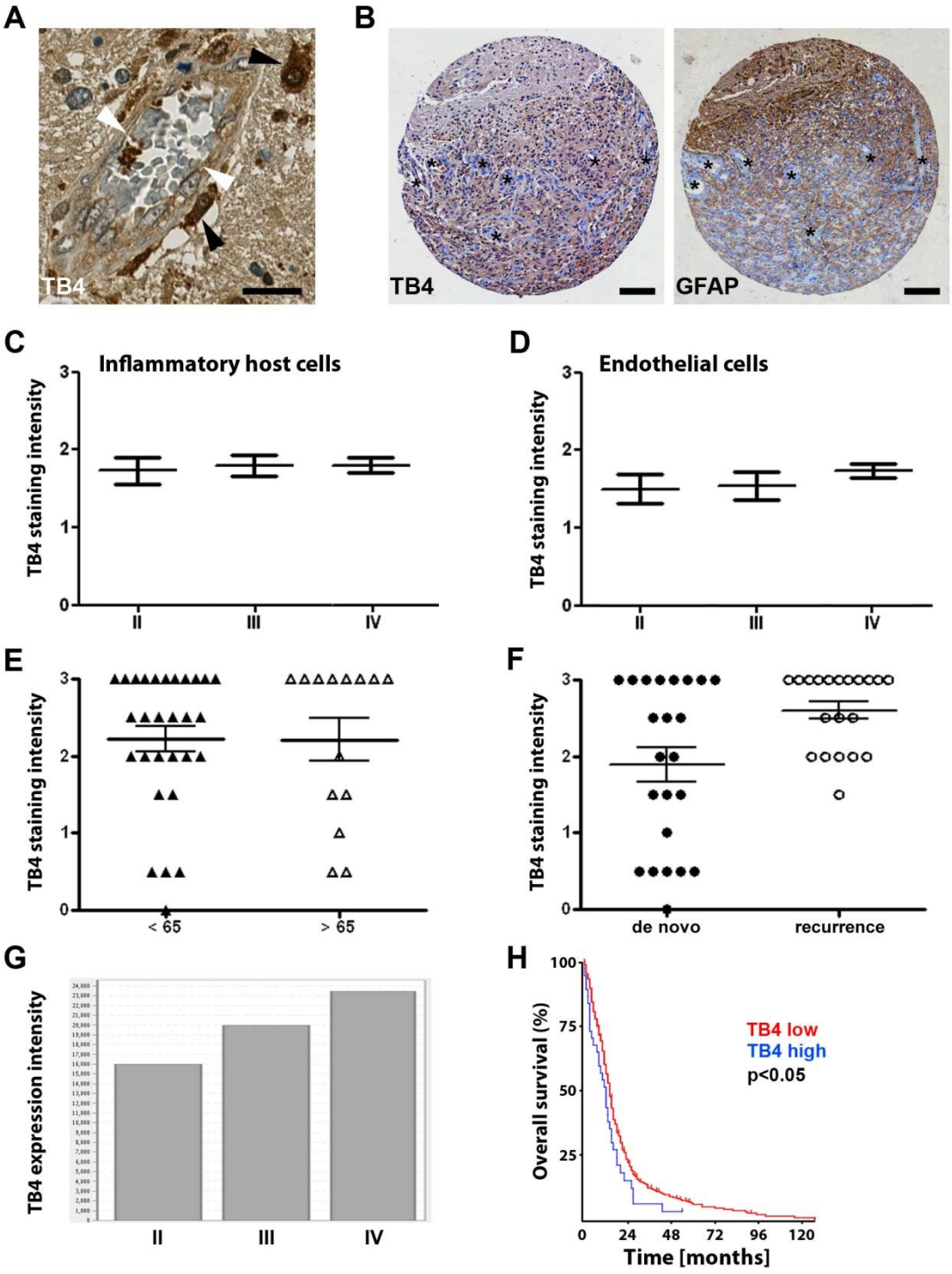

Supplementary Figure 2

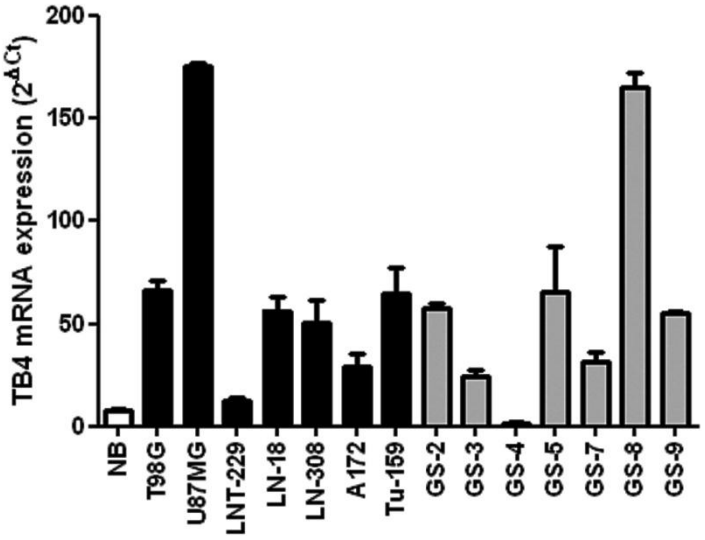

Supplementary Figure 3

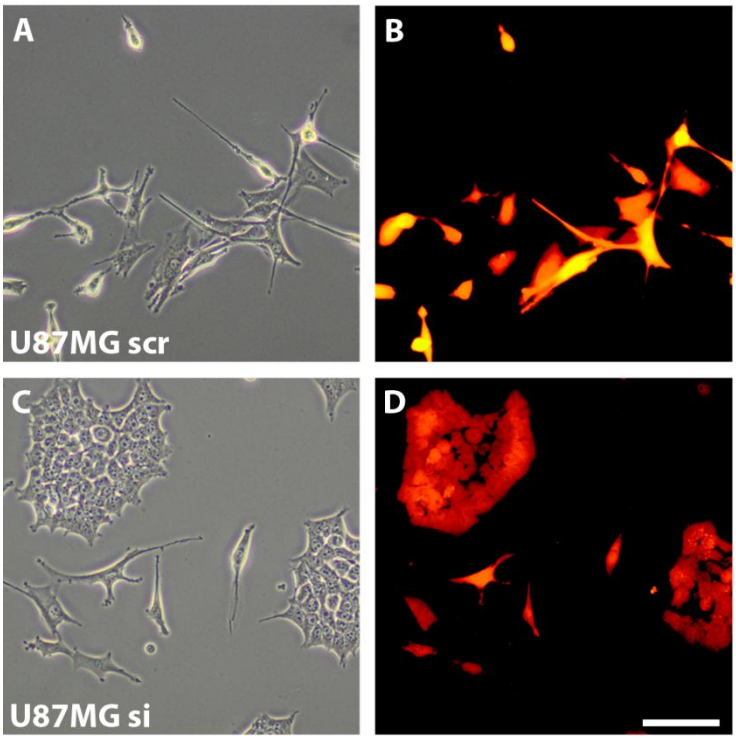

Supplementary Figure 4

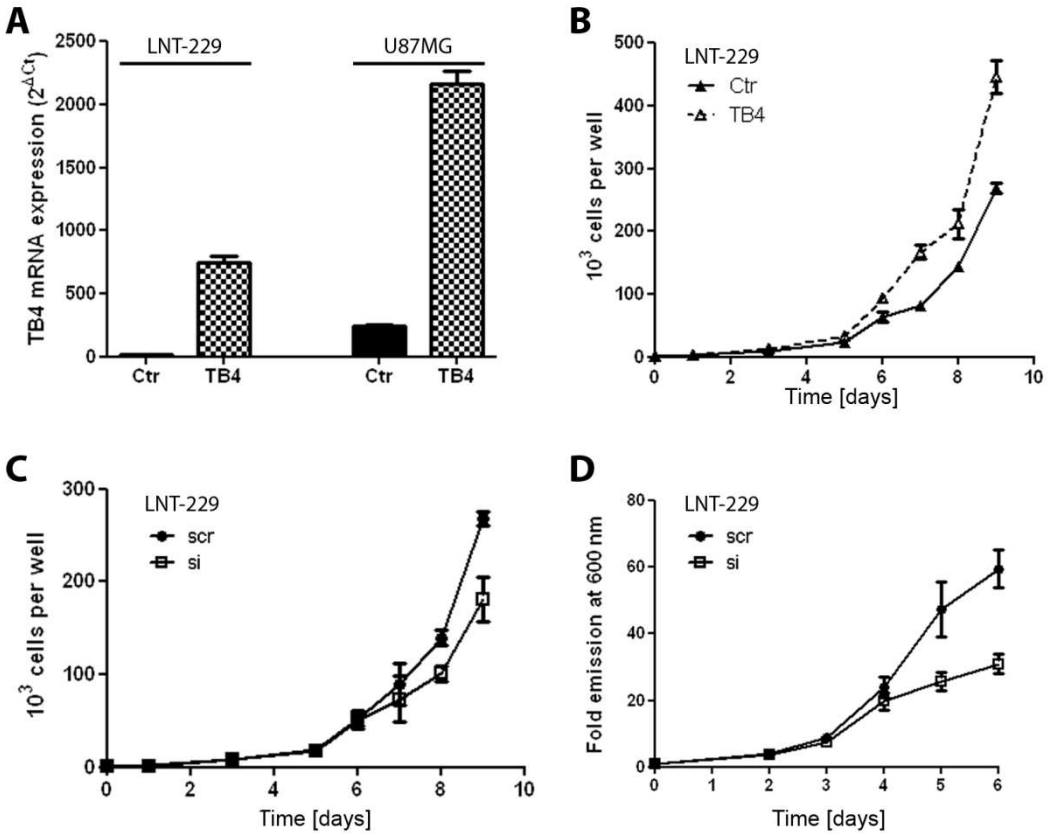

Supplementary Figure 5

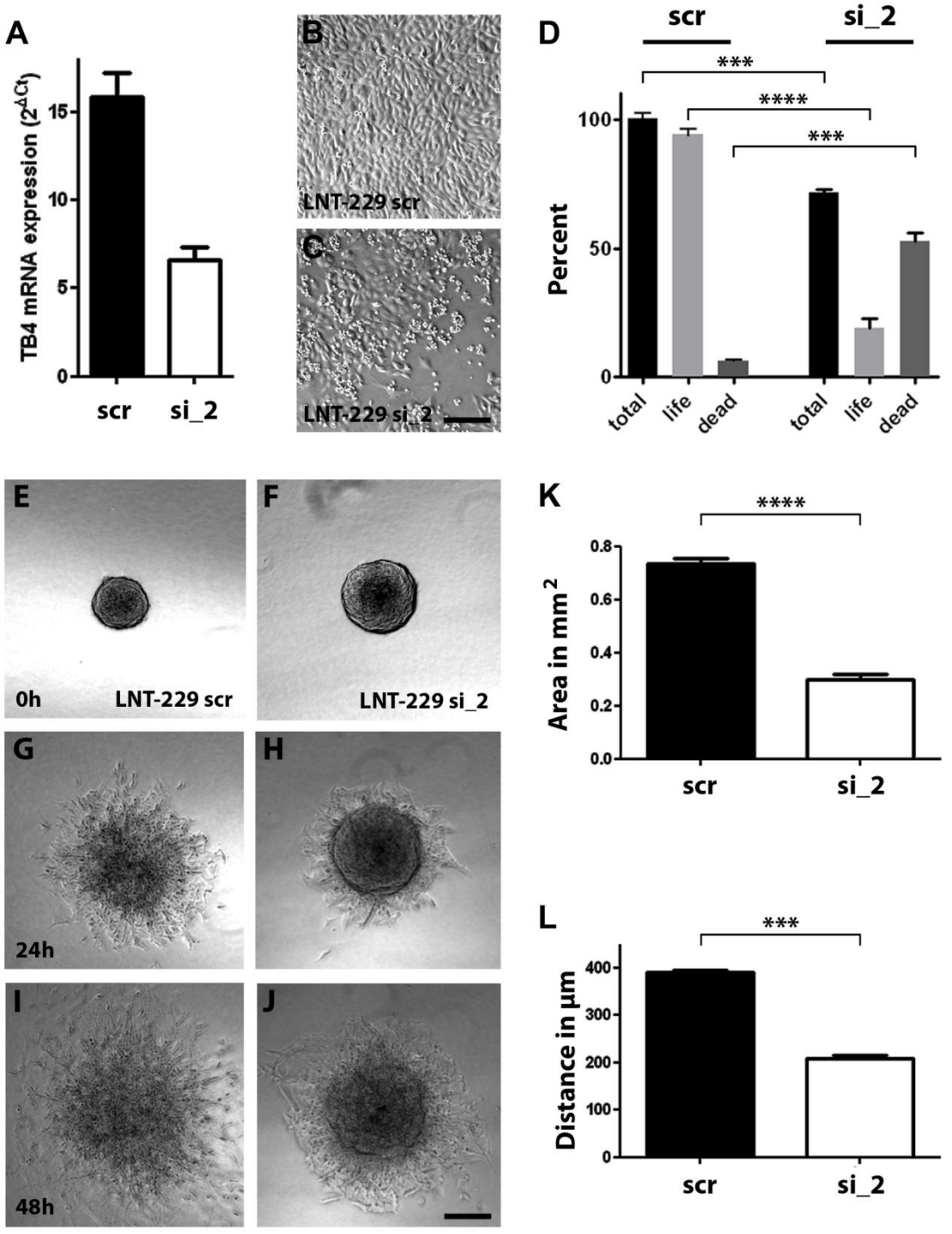

Supplementary Figure 6

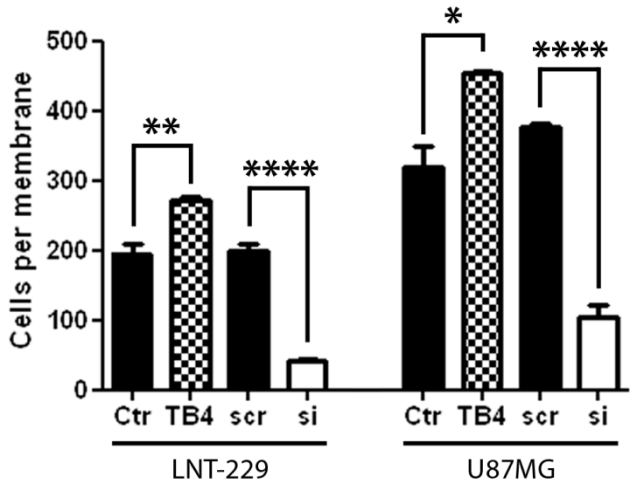

Supplementary Figure 7

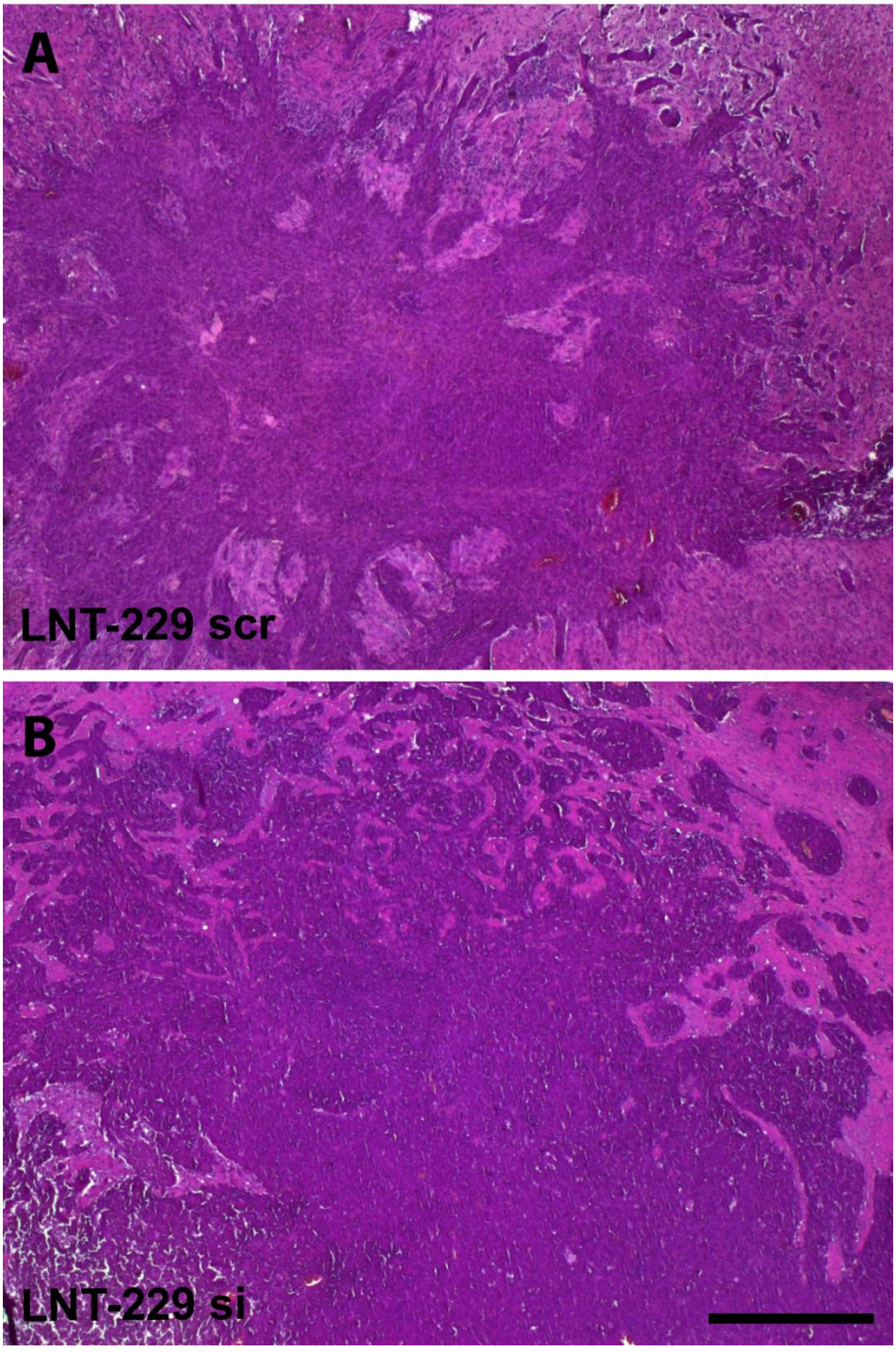

Supplementary Figure 8

A

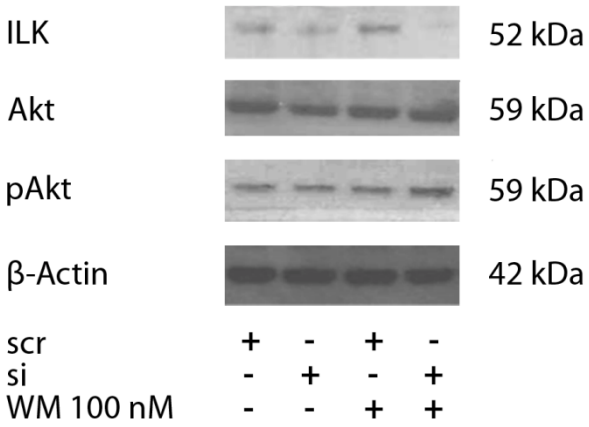

B

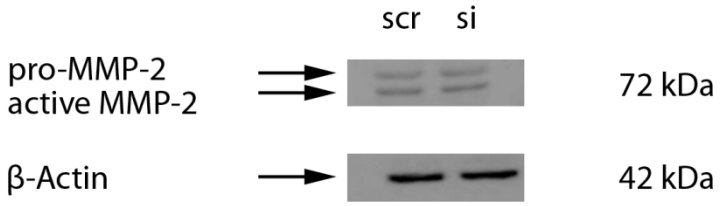

C

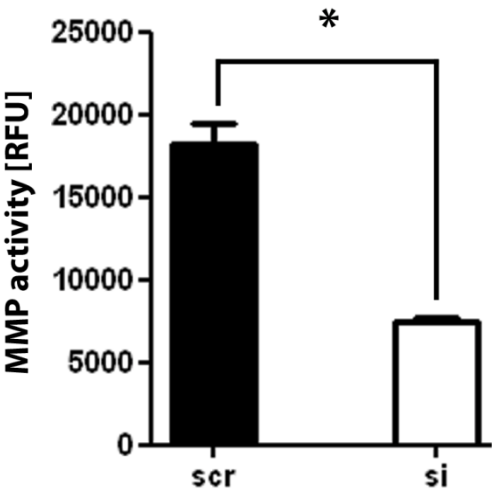

Supplementary Figure 9

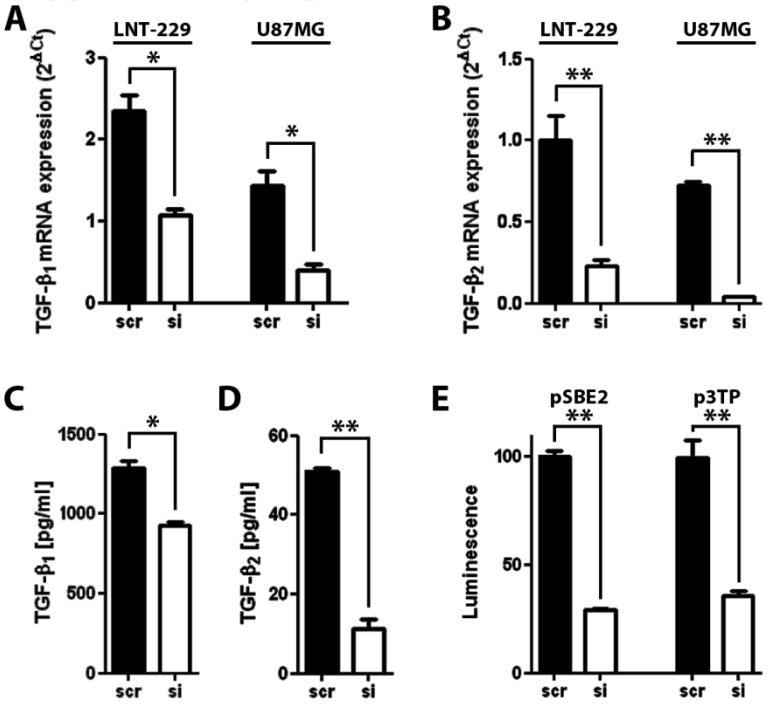

SUPPLEMENTARY TABLE 1

Score	Clinical symptoms in mice
0	no visible impairment, normal gait and behaviour including explorative behaviour in new environment (grid, weighing scale), no steps missed on the grid
1	no visible impairment, normal gait and behaviour including explorative behaviour in new environment (grid, weighing scale), occasional step missed on the grid, reduced activity
2	reduced activity, less motile than healthy animals, reduced explorative behaviour, signs of discomfort (hunched back position, lack of grooming), reduced performance on grid, over one third of steps are missed, 15% weight loss compared to peak weight

SUPPLEMENTARY TABLE 2

No	WHO	Hist	Age	Loc	Res	RTx	TMZ	Other	TB4	Surv
1	II	A	69	Ins, l	P	-	-		1	
2	II	A	52	Tmp, l	P	-	-		3	
3	II	FA	68	Bs	P	-	-		0	57,9
4	II	FA	52	Frt, r	P	-	-		2,5	24,3
5	II	FA	35	Frt-tmp, r	P	-	+		0,5	
6	II	FA	33	Frt, l	P	+	+		1	
7	II	FA	30	Frt, r	T	+	+		2	
8	II	FA	34	Bi-frt	T	+	+		3	
9	II	FA	32	Frt-tmp, l	P	+	+	CCNU	2	
10	II	OD	45	Frt, l	T	-	-		0,5	
11	II	OD	30	Prt, l	P	+	+	CCNU	1	
12	II	OD	30	Frt, r	T	-	-		1	
13	II	OA	61	Frt, r	T	+	-		1,5	6,7
14	II	OA	46	Frt, l	P	+	+		0	
15	II	OA	40	Prt, l	P	-	-		2	
16	II	OA	27	Ins, r	P	-	-		0	
17	II	XA	23	Tmp, l	T	-	-		1,5	
18	III	AA	75	Ins, l	T	+	-		2	7,6
19	III	AA	67	Cng, l	T	+	+		3	13,9
20	III	AA	66	Frt, r	P	+	+		2	15,3
21	III	AA	51	Hpc, l	P	+	-		1	8,7
22	III	AA	41	Frt, l	P	+	+		3	34,4

23	III	AA	43	Tmp-prt-frt, l	P	+	+		1	
24	III	AA	39	Frt, l	T	+	+		2,5	
25	III	AA	37	Hpc, r	P	+	+		1,5	
26	III	AA	38	Occ, r	T	+	+		2	
27	III	AA	37	Tmp, l	P	+	+	BEV, IRI	1	22,8
28	III	AA	30	Ins, r	P	-	-		2	
29	III	AA	24	Frt, l	T	+	+		1	
30	III	AO	73	Frt, r	T	+	+		1,5	6,3
31	III	AO	45	Prt, l	P	+	-		0	
32	III	AO	45	Tmp, r	P	+	-		2,5	
33	III	AO	37	Frt-tmp, r	P	+	+		1	
34	III	AO	26	Ins, l	P	-	+		1	
35	III	AOA	65	Tmp, l	P	+	+		3	
36	III	AOA	57	Frt, l	P	+	+		0	
37	III	AOA	55	Prt, l	P	+	+		1,5	29,2
38	III	AOA	43	Tmp, r	T	+	+		2,5	
39	III	AOA	35	Frt, r	T	+	+		3	
40	III	AOA	33	Frt, l	P	+	+	BEV	1,5	
41	III	GA	54	Hpc, r	P	-	-		1	5,8
42	IV	GBM	25	Prt, l	P	+	-		3	9,9
43	IV	GBM	26	Cng, r	T	-	+	THL	3	11,1
44	IV	GBM	29	Frt, r	P	+	-		1	
45	IV	GBM	29	Tmp, l	T	-	-		3	1,8
46	IV	GBM	30	Tmp, r	P	+	+		0,5	10,7

47	IV	GBM	32	Tmp-prt, l	P	+	+		3	11,5
48	IV	GBM	34	Tmp, l	P	+	+		1,5	7,3
49	IV	GBM	35	Tmp-occ,r	P	+	+		0,5	19,6
50	IV	GBM	37	Tmp, r	T	+	-		3	4,2
51	IV	GBM	37	Tmp, l	T	+	-		3	
52	IV	GBM	38	Tmp-prt, r	T	+	+		3	
53	IV	GBM	40	Tmp, l	P	+	+		2	72,1
54	IV	GBM		Prt, r	P	+	-		1	
55	IV	GBM	41	Tmp, r	T	+	+	CCNU	3	14,8
56	IV	GBM	41	Prt, r	T	-	+	CCNU	2	7,0
57	IV	GBM	44	Frt, l	T	+	+	BEV, IRI	3	16,7
58	IV	GBM	44	Prt-occ, l	T	+	+		3	8,2
59	IV	GBM	46	Tmp, r	P	+	+		2	
60	IV	GBM	48	Tmp, l	T	+	+	BEV, IRI, CCNU	2	27,4
61	IV	GBM	48	Tmp-prt, r	T	-	-		2,5	4,6
62	IV	GBM	48	Tmp, l	T	+	+	BEV	2	18,0
63	IV	GBM	48	Tmp, r	P	+	+	BEV, IRI	2,5	4,8
64	IV	GBM	50	Frt, r	T	+	+	BEV, IRI, CCNU	1,5	14,7
65	IV	GBM	50	Tmp, r	P	+	+		2,5	16,1
66	IV	GBM	51	Tmp, r	P	+	+		3	13,6
67	IV	GBM	52	Tmp, r	T	+	+		3	11,8
68	IV	GBM	52	Tmp-occ,r	T	-	+	GEF	3	32,8
69	IV	GBM	54	Tmp, r	T	+	+		3	10,2
70	IV	GBM	54	Prt-occ, r	T	+	+		1,5	16,5

71	IV	GBM	55	Tmp, r	P	+	+		2,5	9,4
72	IV	GBM	55	Tmp, r	T	+	+		2	16,0
73	IV	GBM	56	Frt, r	T	+	+		0,5	20,0
74	IV	GBM	58	Tmp, l	T	+	+	BEV, IRI	0,5	12,1
75	IV	GBM	61	Hpc, l	P	+	+		3	
76	IV	GBM	61	Prt, r	P	+	+		0	1,8
77	IV	GBM	64	Frt, l	P	+	+		0,5	
78	IV	GBM	66	Bi-frt	P	+	+		3	8,5
79	IV	GBM	69	Frt, l	P	+	+	THL, GEF	2,5	109,5
80	IV	GBM	74	Prt-tmp, r	P	+	+	PRC, CCNU, VIN, GEF	3	48,2
81	IV	GBM	83	Tha, l	P	+	+	BEV, CCNU	2	22,2
82	IV	GBM	83	Frt, l	P	+	+	CCNU, GEF, BEV, IRI	3	32,1
83	IV	GBM	88	Tmp	P	+	+		2	4,1
84	IV	GBM (AOA)	59	Tmp	T	+	+		0,5	
85	IV	GBM (AOA)	38	Prt	P	+	+	GEF, THL	2	
86	IV	GBM (OA)	30	Frt-tmp, r	P	+	+		3	12,7
87	IV	GSR	35	Frt, r	T	-	-		3	15,7
88	IV	GSR	37	Tmp, l	P	+	+		1,5	3,4
89	IV	GSR	51	Prt, r	P	+	-		2,5	15,1

SUPPLEMENTARY TABLE 3

Transcription factors					
up-regulated			down-regulated		
Probe Set ID	Fold change	Gene Symbol	Probe Set ID	Fold change	Gene Symbol
222171_s_at	34,90	PKNOX2	213139_at	24,75	SNAI2
219778_at	30,02	ZFPM2	243456_at	12,07	ZNF214
211181_x_at	16,54	RUNX1	204236_at	7,18	FLI1
63305_at	12,88	PKNOX2	228915_at	5,49	DACH1
211182_x_at	11,30	RUNX1	228716_at	4,47	THRB
206261_at	7,92	ZNF239	205472_s_at	4,38	DACH1
208502_s_at	7,74	PITX1	209242_at	4,27	PEG3
207397_s_at	6,09	HOXD13	230472_at	4,17	IRX1
226267_at	5,72	JDP2	209243_s_at	4,15	PEG3
206377_at	5,55	FOXF2	209348_s_at	4,05	MAF
236681_at	5,48	HOXD13	202672_s_at	4,04	ATF3
1569191_at	5,13	ZNF826	201331_s_at	3,83	STAT6
213006_at	4,37	CEBPD	206837_at	3,76	ALX1
228462_at	3,94	IRX2	201693_s_at	3,75	EGR1
226806_s_at	3,42	NFIA	209189_at	3,62	FOS
203973_s_at	3,40	CEBPD	229657_at	3,58	THRB
229638_at	3,29	IRX3	207144_s_at	3,56	CITED1
205932_s_at	3,15	MSX1	201694_s_at	3,44	EGR1
226590_at	3,14	ZNF618	203554_x_at	3,30	PTTG1
221016_s_at	3,09	TCF7L1	205249_at	3,29	EGR2

242939_at	2,93	TFDP1	228170_at	3,24	OLIG1
204798_at	2,82	MYB	1559942_at	3,22	MDFIC
203408_s_at	2,81	SATB1	226255_at	3,18	ZBTB33
230438_at	2,78	TBX15	208216_at	3,11	DLX4
204914_s_at	2,74	SOX11	207828_s_at	3,11	CENPF
238977_at	2,74	MCM6	227261_at	2,99	KLF12
203787_at	2,72	SSBP2	230068_s_at	2,95	PEG3
1553172_at	2,70	ZNF777	209172_s_at	2,90	CENPF
226695_at	2,68	PRRX1	226680_at	2,87	IKZF5
201502_s_at	2,68	NFKBIA	226680_at	2,87	IKZF5
238444_at	2,67	ZNF618	209357_at	2,80	CITED2
209538_at	2,67	ZNF32	205471_s_at	2,78	DACH1
210697_at	2,66	ZNF257	228999_at	2,68	CHD2
223915_at	2,65	BCOR	203556_at	2,62	ZHX2
232546_at	2,58	TP73	218849_s_at	2,60	PPP1R13L
223916_s_at	2,56	BCOR	206029_at	2,60	ANKRD1
210829_s_at	2,49	SSBP2	213293_s_at	2,59	TRIM22
204915_s_at	2,48	SOX11	228038_at	2,51	SOX2
209587_at	2,46	PITX1	203874_s_at	2,50	SMARCA1
229956_at	2,44	NR2C1	214276_at	2,49	KLF12
207179_at	2,44	TLX1	226420_at	2,45	EVI1
224975_at	2,43	NFIA	207401_at	2,45	PROX1
230511_at	2,42	CREM	235308_at	2,41	ZBTB20
206915_at	2,41	NKX2-2	221234_s_at	2,40	BACH2

209392_at	2,34	ENPP2	204790_at	2,38	SMAD7
204913_s_at	2,34	SOX11	227404_s_at	2,36	EGR1
228200_at	2,34	ZNF252	232641_at	2,36	ZNF596
236471_at	2,29	NFE2L3	209505_at	2,34	NR2F1
226484_at	2,28	ZBTB47	206848_at	2,34	HOXA7
221350_at	2,27	HOXC8	202761_s_at	2,29	SYNE2
224976_at	2,26	NFIA	209383_at	2,28	DDIT3
210530_s_at	2,24	NR2C1	202221_s_at	2,28	EP300
226461_at	2,23	HOXB9	201746_at	2,27	TP53
226592_at	2,22	ZNF618	215294_s_at	2,27	SMARCA1
234055_s_at	2,21	GZF1	203875_at	2,25	SMARCA1
223586_at	2,20	ARNTL2	236645_at	2,21	HBP1
224970_at	2,20	NFIA	229881_at	2,21	KLF12
205991_s_at	2,19	PRRX1	208960_s_at	2,18	KLF6
221703_at	2,17	BRIP1	222830_at	2,17	GRHL1
204791_at	2,16	NR2C1	238940_at	2,16	KLF12
218866_s_at	2,15	POLR3K	213413_at	2,16	STON1
230440_at	2,14	ZNF469	205383_s_at	2,15	ZBTB20
210061_at	2,14	ZNF589	238231_at	2,15	NFYC
204039_at	2,13	CEBPA	215111_s_at	2,15	TSC22D1
206601_s_at	2,12	HOXD3	204622_x_at	2,14	NR4A2
239911_at	2,12	ONECUT2	216248_s_at	2,14	NR4A2
202986_at	2,11	ARNT2	1554980_a_at	2,13	ATF3
239412_at	2,11	IRF5	204621_s_at	2,13	NR4A2

210062_s_at	2,08	ZNF589	235520_at	2,10	ZNF280C
1558722_at	2,08	ZNF252	228125_at	2,10	ZNF397OS
233446_at	2,04	ONECUT2	226991_at	2,09	NFATC2
209710_at	2,04	GATA2	244743_x_at	2,09	ZNF138
204702_s_at	2,03	NFE2L3	209054_s_at	2,08	WHSC1
202490_at	2,02	IKBKAP	207069_s_at	2,08	SMAD6
222921_s_at	2,01	HEY2	202414_at	2,07	ERCC5
210531_at	2,00	NR2C1	223704_s_at	2,07	DMRT2
			1555832_s_at	2,06	KLF6
			232529_at	2,06	SP3
			242433_at	2,04	ZBTB11
			232231_at	2,03	RUNX2
			205460_at	2,03	NPAS2
			40560_at	2,03	TBX2
			224606_at	2,02	KLF6
			233175_at	2,01	ZNF460
			216279_at	2,01	ZNF460
			1562245_a_at	2,00	ZNF578

SUPPLEMENTARY TABLE 4

Gene ontology Migration					
up-regulated			down-regulated		
Probe Set ID	Fold change	Gene Symbol	Probe Set ID	Fold change	Gene Symbol
202638_s_at	6,08	ICAM1	203325_s_at	6,44	COL5A1
242517_at	5,91	KISS1R	226534_at	4,67	KITLG
39402_at	5,35	IL1B	214702_at	3,59	FN1
202637_s_at	4,30	ICAM1	204035_at	3,29	SCG2
205067_at	4,13	IL1B	214701_s_at	3,19	FN1
204351_at	3,85	S100P	1558199_at	3,07	FN1
204563_at	3,27	SELL	212489_at	2,85	COL5A1
212143_s_at	2,90	IGFBP3	203989_x_at	2,84	F2R
210095_s_at	2,71	IGFBP3	209357_at	2,80	CITED2
209355_s_at	2,71	PPAP2B	209909_s_at	2,73	TGFB2
204844_at	2,70	ENPEP	204105_s_at	2,50	NRCAM
223454_at	2,65	CXCL16	204105_s_at	2,50	NRCAM
215240_at	2,48	ITGB3	204105_s_at	2,50	NRCAM
212230_at	2,45	PPAP2B	201108_s_at	2,46	THBS1
203381_s_at	2,39	APOE	204790_at	2,38	SMAD7
209946_at	2,36	VEGFC	209505_at	2,34	NR2F1
204995_at	2,28	CDK5R1	235086_at	2,28	THBS1
215485_s_at	2,26	ICAM1	229114_at	2,25	GAB1
218629_at	2,16	SMO	212298_at	2,24	NRP1
204363_at	2,14	F3	201109_s_at	2,19	THBS1

239911_at	2,12	ONECUT2	212488_at	2,19	COL5A1
213030_s_at	2,05	PLXNA2	202803_s_at	2,18	ITGB2
233446_at	2,04	ONECUT2	239233_at	2,17	CCDC88A
			212144_at	2,14	UNC84B
			225806_at	2,11	JUB
			1553764_a_at	2,08	JUB
			210495_x_at	2,06	FN1
			212464_s_at	2,06	FN1
			216442_x_at	2,02	FN1

SUPPLEMENTARY TABLE 5

Gene ontology Apoptosis					
up-regulated			down-regulated		
Probe Set ID	Fold change	Gene Symbol	Probe Set ID	Fold change	Gene Symbol
216598_s_at	11,73	CCL2	202036_s_at	7,46	SFRP1
204933_s_at	7,85	TNFRSF11B	218499_at	7,36	RP6-213H19.1
205681_at	7,74	BCL2A1	202037_s_at	7,36	SFRP1
215223_s_at	7,36	SOD2	203139_at	6,62	DAPK1
1566342_at	6,07	SOD2	202035_s_at	5,92	SFRP1
204932_at	5,98	TNFRSF11B	226534_at	4,67	KITLG
216841_s_at	5,80	SOD2	209242_at	4,27	PEG3
210538_s_at	5,80	BIRC3	209243_s_at	4,15	PEG3
39402_at	5,35	IL1B	209031_at	3,81	CADM1
203528_at	5,05	SEMA4D	1554264_at	3,74	CKAP2
221477_s_at	4,72	SOD2	209032_s_at	3,59	CADM1
228153_at	4,46	RNF144B	204035_at	3,29	SCG2
205067_at	4,13	IL1B	224985_at	2,97	NRAS
204224_s_at	4,12	GCH1	230068_s_at	2,95	PEG3
227143_s_at	3,96	BID	203989_x_at	2,84	F2R
204513_s_at	3,86	ELMO1	209357_at	2,80	CITED2
210118_s_at	3,77	IL1A	203373_at	2,75	SOCS2
204493_at	3,59	BID	209909_s_at	2,73	TGFB2
202643_s_at	3,28	TNFAIP3	237107_at	2,70	PRKRAP1
202644_s_at	3,16	TNFAIP3	209030_s_at	2,61	CADM1

205932_s_at	3,15	MSX1	218849_s_at	2,60	PPP1R13L
205047_s_at	3,07	ASNS	201291_s_at	2,47	TOP2A
212143_s_at	2,90	IGFBP3	201108_s_at	2,46	THBS1
1554830_a_at	2,83	STEAP3	230380_at	2,41	THAP2
211725_s_at	2,81	BID	202512_s_at	2,40	ATG5
210095_s_at	2,71	IGFBP3	204790_at	2,38	SMAD7
233011_at	2,68	ANXA1	223349_s_at	2,35	BOK
201502_s_at	2,68	NFKBIA	221478_at	2,33	BNIP3L
232546_at	2,58	TP73	201292_at	2,29	TOP2A
211475_s_at	2,56	BAG1	209383_at	2,28	DDIT3
216252_x_at	2,44	FAS	235086_at	2,28	THBS1
212196_at	2,41	IL6ST	202221_s_at	2,28	EP300
218424_s_at	2,40	STEAP3	201746_at	2,27	TP53
203381_s_at	2,39	APOE	203372_s_at	2,23	SOCS2
215719_x_at	2,37	FAS	205858_at	2,23	NGFR
216705_s_at	2,34	ADA	225858_s_at	2,22	XIAP
204995_at	2,28	CDK5R1	237469_at	2,20	TOP2A
204863_s_at	2,25	IL6ST	201109_s_at	2,19	THBS1
213257_at	2,20	SARM1	223257_at	2,18	G2E3
221583_s_at	2,20	KCNMA1	202803_s_at	2,18	ITGB2
204639_at	2,18	ADA	206189_at	2,17	UNC5C
218629_at	2,16	SMO	228363_at	2,13	XIAP
212195_at	2,16	IL6ST	1555675_at	2,08	BLID
211450_s_at	2,15	MSH6	207069_s_at	2,08	SMAD6

204363_at	2,14	F3	202414_at	2,07	ERCC5
218627_at	2,11	DRAM	221479_s_at	2,04	BNIP3L
211000_s_at	2,10	IL6ST	223254_s_at	2,01	G2E3
207199_at	2,09	TERT			
207536_s_at	2,09	TNFRSF9			
1552519_at	2,08	ACVR1C			
223322_at	2,06	RASSF5			
203619_s_at	2,05	FAIM2			
218380_at	2,05	NLRP1			
220999_s_at	2,05	CYFIP2			
204352_at	2,04	TRAF5			

SUPPLEMENTARY TABLE 6

Verhaak et al. 2010 up-regulated / down-regulated					
Proneural		Mesenchymal		Classical	
up	down	up	down	up	down
CLGN	SLC2A10	BNC2	CDK5R1	ELOVL2	PGBD5
PDE10A	DRAM	COL1A1	MAPT	SMO	TPM3
LPHN3	ANXA1	CTSC	ANKRD46	TLE2	ENPP4
NKX2-2	FZD7	CSTA	CLASP2	MYO10	ARRB1
SATB1	GJA1	TRPM2	SOX2	CDK6	ENPP2
SOX11	ARSJ	ACPP	MAP2	FGFR3	SYNGR2
FLRT1	PLS3	TNFAIP3	CKB	SOCS2	EDIL3
MYB	TRIM22	BDKRB2	TSPAN3	LFNG	GNAI1
MCM10		AIM1		KLHL4	ACSL4
CDC25A		COL5A1			
HOXD3		COL1A2			
ALCAM		THBS1			
FHOD3		NRP1			
FAM110B		SLC16A3			
HMGB3		DAB2			
MARCKS		DSE			
BCOR		LAPTM5			
		ITGB2			
		STAT6			

RUNX2

SUPPLEMENTARY TABLE 7

Carro et al. 2010 up-regulated / down-regulated		
Proneural	**Mesenchymal**	**Proliferative**
SCD	IFITM2	MCM6
GABBR1	ICAM1	RAD51
APOE	FBN1	CCNE2
MAPT	TAGLN	GINS1
ALDH5A1	RUNX1	ARNTL2
FAIM2	CA12	TIFA
ELMO1	C1R	ITGA2
BMP2	STEAP3	NPHP1
MAPT	PAPPA	DLGAP5
FLRT1	METTL7B	AURKA
SLITRK5	SPOCD1	NEK2
CYFIP2	SLC16A3	TOP2A
FERMT1	LPAR1	NDC80
HEY2	NRP1	CKS2
RASSF4	COL4A1	TTK
PKNOX2	COL4A2	CENPA
NTN4	PELO	CENPE
TMOD2	SHROOM3	CDC25C
LOC202451	EMP1	KIF14
KSR2		HMMR

FGF13	CENPF
OMG	BUB1
MAF	MDFIC
ZCCHC24	CCNB1
FAM110B	ECT2
IKZF5	ASPM
OLIG1	NUSAP1
NALCN	KIF18A
RPL13	NUF2
CNTN3	SPIN4
FAM133A	SGOL2
FSTL5	hCG_181549

SUPPLEMENTARY TABLE 8

Cahoy et al. 2008			
up-regulated / down-regulated			
Astrocyte		Oligodendrocyte	
up	down	up	down
OMG	MARCKS	TTYH2	F2R
NPAS2	PDZRN3	DBNDD2	FSTL5
RHOU	FSTL5	PARVB	MKI67
	EGR2	APOD	LPHN3
	NR4A2		SOX11
	GAS2L3		
	CENPA		
	CDCA8		
	ECT2		
	PRC1		
	CEP55		
	TOP2A		
	MKI67		
	CKS2		
	CCNB2		
	BUB1		
	CENPF		
	CCNB1		
	H19		

EMP1

MCM6

PTX3